Geometric Modeling of Rainfall Fields

By
Carlos E. Puente
Hydrologic Science
Department of Land, Air and Water Resources
University of California, Davis
Davis, CA 95616

TECHNICAL COMPLETION REPORT
Project Number UCAL-WRC-W-804
August, 1995

University of California Water Resources Center

The research leading to this report was supported by the University of California Water Resources Center, as part of Water Resources Center Project UCAL-WRC-W-804.

Abstract

Accurate rainfall modeling is of vital importance for the proper management of our environment. Rainfall descriptions are required, among others, to model pollution migration, to address issues related to climate change (i.e. global circulation), to estimate extreme weather events, and to manage our watersheds. Adequate environmental planning can only be accomplished with reliable rainfall quantification. Even though several sophisticated (stochastic) rainfall models exist, they do not capture all the variability observed at a fixed location when a storm passes by. Typical models approximate the irregular and intermittent rain patterns (of a fractal and/or multifractal nature) by superimposing randomly arriving smooth Euclidean objects (i.e. rectangular pulses), and consequently preserve only some statistical features of the rainfall series (fields) (e.g. mean, variance, spatial correlations, etc.). Since these representations are typically limited by their analytical tractability and because there has been a recognition of chaotic effects in rainfall, a new approach for rainfall modeling based on multinomial multifractal measures and fractal interpolating functions has been developed by Puente (1992, 1995). The basis for these fractal-multifractal models is the fact that predictability could only be improved when the observed (intermittent) details present in rainfall events are considered explicitly. One advantage of the fractal geometric procedure is that its outcomes are entirely deterministic. This follows because the two components that make up the approach are deterministic.

This work reports on the use of the new models to represent: (i) high resolution rainfall time series, (ii) natural processes of two kinds, namely those termed chaotic or stochastic, and (iii) spatial rainfall (geophysical) patterns. In relation to the high resolution rainfall, it is shown that the intrinsic shape and variability of three storms gathered every few seconds (5 to 15) may be captured employing the fractal geometric methodology. It is illustrated how these data sets are parsimoniously encoded wholistically, resulting in very faithful descriptions of both major trends and small (noisy) fluctuations. These results suggest that a stochastic framework for rainfall may not be required. In regards to the geometric description of general natural time series, it is exhibited via simulations that the fractal-multifractal approach does provide a convenient framework to describe a large class of records that would pass, according to typical statistical and chaotic criteria, as low-dimensional and chaotic or as high-dimensional and stochastic. In order to handle rainfall (radar reflectivities) patterns in space, extensions of the fractal-multifractal procedure to higher dimensions are also included. The potential for the development of a new approach to rainfall dynamics in space, based on the geometric features of spatial patterns, is discussed.

Key words: rainfall modeling, turbulence, intermittency, fractal geometry, multifractals, projections.

Contents

List of Tables

List of Figures

1 Problem and Research Objectives

This work addresses the problem of understanding the intermittent structure that rainfall records exhibit. Although several representations for rainfall exist, the most sophisticated stochastic models only preserve some statistics of the available records, and consequently do not capture the specific details present in them. The overall objective of this research is the development of a framework for the proper quantification of natural intermittent phenomena, and in particular rainfall.

An introduction to the recent literature which suggested the possibility of developing a new approach to rainfall is given next. Afterwards, a description of the most common rainfall models is included.

1.1 Basis For a New Approach

A new vision to understand the intricacies of physical phenomena has been gained with the advent of the modern theory of turbulence (chaos) and fractal geometry. In this relation, three important paradigms have appeared:

(a) Details that were thought to be unimportant may in fact play crucial roles in our ability to predict; e.g. Lorenz (1963), Moon (1987).

(b) What appears unpredictable and "random" at a local scale could be explained as part of a global deterministic process; e.g. Lorenz (1963), Mandelbrot (1983), Meneveau and Sreenivasan (1987).

(c) Very complicated processes, which were thought to require partial differential equations for their description (e.g. convection, fully-developed turbulence), may be accurately described by means of very simple deterministic models; e.g. Libchaber (1982), Meneveau and Sreenivasan (1987), Feigenbaum (1980).

The framework provided by these paradigms constitutes the basis herein. The specific applications to Hydrology are inspired in part by the call to new approaches to the science, as suggested by Dooge (1986).

Understanding hydrologic (geophysical) phenomena requires the proper quantification (interpolation, estimation, prediction, simulation, etc.) of the available information in time and in space. This is a difficult task because these data sets are *complex*. They exhibit heterogeneities, anisotropies, and intermittencies which preclude their simple mathematical description. The typical approach for many years has been to understand such variability based upon well founded physical principles, i.e. partial differential equations which express conservation laws, e.g. Eagleson (1970), Freeze and Cherry (1979), and to quantify the remaining uncertainties due to our imperfect knowledge via probability theory, e.g. Bras and Rodriguez-Iturbe (1985), Bhattacharya and Gupta (1990), and Cressie (1991).

Given the inherent difficulties in fully describing the complex data sets we have available and the fact that often times such data is not completely accurate, many stochastic procedures center their attention on relevant statistics of the patterns at hand (i.e. means,

variances, spatial correlations, extremes, etc.) and employ assumptions like stationarity (homogeneity) and ergodicity in order to develop manageable theories. Despite substantial progress throughout the years, the problem of "spatial variability" is still an important limitation in several geophysical disciplines and the development of new methods is needed, see Dooge (1986) and NRC (1991a, b). Although state of the art stochastic methods may provide a viable representation for complex data, the simplifying assumptions used may lead to smoothed and/or distorted representations of the observed data sets. This may happen also because preservation of some relevant statistics do not necessarily translate into preservation of whole geometrical patterns. The paradigms above suggest that not being able to capture the geometric details of our data sets may hamper our ability to predict, specially if the prevailing dynamic conditions are sufficiently nonlinear.

Descriptions of natural phenomena via fractal geometry have been developed and popularized by Mandelbrot (1983, 1989). The basic assumption is that the underlying process possesses a geometric structure that repeats when looked at increasingly smaller scales. This self-similarity (self-affinity) represents a plausible way for bridging the gap across alternative scales, and has been found of relevance in several disciplines in Physics, e.g. Mandelbrot (1983), Feder (1988). Lately, these ideas have played an important role in the ever intriguing field of turbulence. In fact, the use of multifractal measures, e.g. Meneveau and Sreenivasan (1987) and Sreenivasan (1991), appears to provide an adequate framework to study the very intermittent and highly heterogeneous behavior observed in turbulence. It is worth mentioning that even though the power of fractal ideas is unquestionable, a couple of common objections have been that: (i) the use of the most simple mathematical fractals give rise to self-similarity (self-affinity) ad-infinitum, a property hardly observed with real (geophysical) data; and (ii) the use of fractal techniques sometimes is not properly linked with the "Physics" of the underlying phenomena.

In this work, a new procedure for the quantification of space-time variability of hydrologic (geophysical) phenomena is reviewed and used. The idea is to reproduce the "complex", "jagged", and "intricate" hydrologic patterns as deterministic fractal transformations of turbulence-related distributions (multifractal probability measures). The transformations to be used belong to the family of deterministic continuous fractal interpolating functions, as introduced by Barnsley (1986) and Barnsley et al. (1989). It will be shown that this approach provides a compact quantification of high resolution rainfall records, which may lead to better understanding of the underlying phenomena. It is illustrated via simulations that they may also result in improved dynamic representations of hydrologic (geophysical) processes.

1.2 Literature Review

A brief summary of pertinent research on rainfall modeling is presented here. This is included to stress the advantages and disadvantages of these models, and to contrast their scope with the proposed methodology. No detailed description is given to "physically-based" models (e.g. Georgakakos and Bras (1984) or alike). Instead this section concentrates on stochastic and fractal models.

Many stochastic models for rainfall at a site have been reported in the literature. They

differ in their assumed distributions of: (i) rainfall arrivals, and (ii) rainfall produced at each instance. Typically, rainfall is computed superimposing all contributions from "cells" occurring before the time of interest. Rectangular pulses with random intensities and durations are the most typical parameterization. Early models assumed an homogeneous Poisson description for the arrivals. Representative among these approaches are the works of Todorovic (1968), Gupta (1973), Eagleson (1978), and Marien and Vandewielde (1986). Non-homogeneous Poisson (Cox) models have also been reported, i.e. Smith and Karr (1983), Guttorp (1986). To account for the observed clustering (intermittency) of rainfall events, schemes that replace the Poisson arrivals have been developed. The use of the Neyman-Scott clustering representation is illustrated in the works of Kavvas and Delleur (1981), Waymire and Gupta (1981), Rodriguez-Iturbe et al. (1984), Rodriguez-Iturbe (1986). An approach based on randomized Bernoulli trials is given by Smith (1987). The use of the Bartlett-Lewis clustering model is reported in the work of Rodriguez-Iturbe (1987a).

Comparisons among some of these models have been carried. It has been found that cluster-based procedures are better than Poisson-based ones (Valdes et al. (1985), Rodriguez-Iturbe et al. (1987b)), but inconsistencies have been observed in cluster models regarding their ability to have a unique set of parameters irrespectively of the degree of aggregation, Foufoula-Georgiou and Guttorp (1986). Although progress has been made on parameter estimation (Smith and Karr (1985)), no single model is universally accepted for a given situation.

In summary, stochastic rainfall models at a spatial location try to mimic the structure observed on storms at a site. The way information is synthesized is by means of statistical quantities (mean arrival rates, mean storm duration and intensity, spectrum of counts, etc.). Although simulated series do preserve statistical characteristics like mean, variance, and some autocorrelations, global capturing of rainfall (i.e. the observed details and the implied probability distribution) is not accomplished. Being based on average quantities and simplified conditions to ensure mathematical tractability, these models are typically limited in their ability to perform well at extreme events.

A new brand of model was introduced by considering rainfall as a chaotic process, Rodriguez-Iturbe et al. (1989). Even though determinism becomes an important component of the approach, actual dynamic modeling (i.e. finding the equations of motion from a time series) is quite difficult (e.g. Crutchfield and McNamara (1987), Casdagli (1989)), and limits the practical applicability of the otherwise beautiful methodology. A "fractal" representation to rainfall was introduced by Lovejoy and Schertzer (1985, 1990), and Schertzer and Lovejoy (1987) via the notion of universal multifractals. Their idea is to represent rainfall (and other geophysical processes) as a realization of a Levy stochastic process, and parameterize it via its codimension function (a portion of the multifractal spectrum, e.g. Feder, 1988). Success has been attained in characterizing such function for alternative data sets, e.g. Lovejoy and Schertzer (1990). Even though reasonably looking simulations may be obtained, it is difficult to find conditional simulations with such an approach.

In this work, rainfall time series are modeled via fractals and multifractals. An important difference between the fractal-multifractal approach and those just mentioned is that the former is entirely deterministic. As will be explained later on, no assumptions regarding

stationarity or ergodicity are needed. As can be seen in Figures 8, 9, 10 and 14, the fractal-multifractal representation results in "random-looking" outcomes which are not random at all. And for the proper combinations of parameters they indeed "look" and have the statistical characteristics of actual rainfall records. This includes statistical properties preserved by the aforementioned stochastic models and, in particular, the codimension function and chaotic characteristics present in the data (Puente and Lobato, 1994, Puente and Juliao, 1994, Puente and Obregón, 1995).

2 Methodology: The Fractal-Multifractal Approach

The fractal-multifractal approach of Puente (1992, 1994, 1995) is reviewed next. Included first is a geometric description of the procedure followed by mathematical treatments of fractal interpolators in two and three dimensions. The section ends with a brief summary of multifractal statistics.

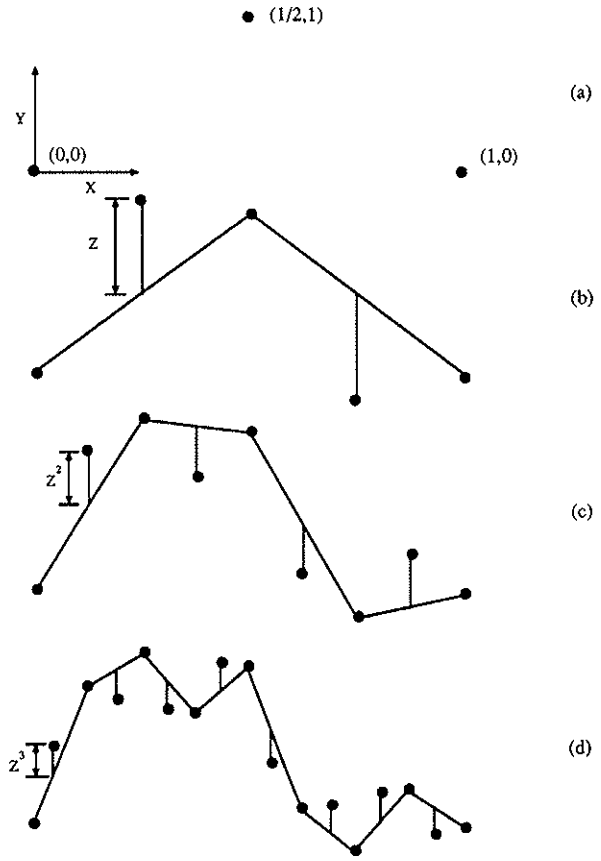

Figure 1: Recursive construction of fractal interpolating function.

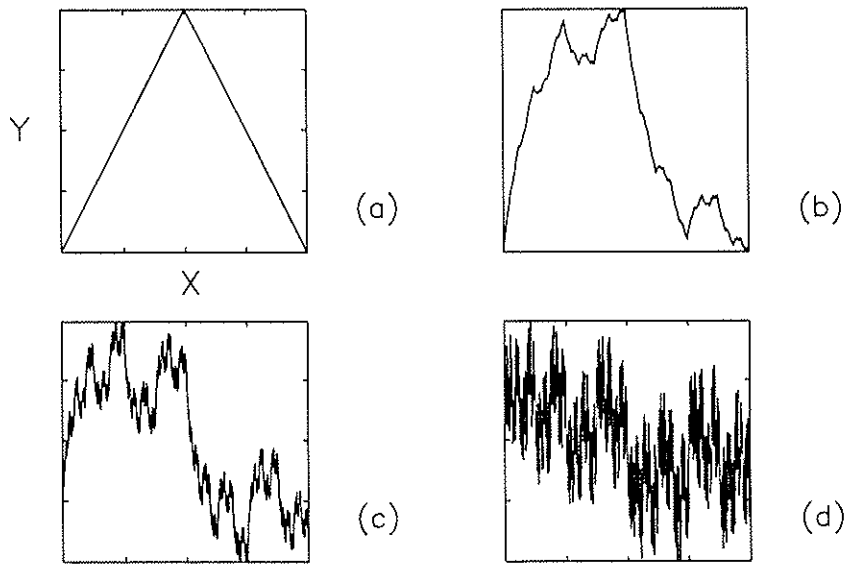

Figure 2: Examples of fractal interpolators: (a) $z = 0$, (b) $z = 0.45$, (c) $z = 0.7$, (d) $z = 0.995$.

2.1 Fractal Interpolation, Multifractals and Derived Measures

Consider the set of three data points $\{(0,0),(0.5,1),(1,0)\}$ (equally spaced in x) as illustrated in Figure 1(a). Fix a real number $0 \leq z < 1$, draw lines between the points and locate two intermediate points going up and down the distance z from the mid-points of the line segments, as shown in Figure 1(b). Continue the process by joining the newly acquired points and the original ones, locating four additional intermediate points (in the middle of the line segments) by going up, down, and down, up respectively a distance z^2, as shown in Figure 1(c). Carry the process ad-infinitum, adding at the n-th stage 2^n intermediate points with vertical displacements of magnitude z^n. Take displacements at stage n those of stage $n-1$ on the first half, and the reciprocal of these on the second half. For instance, in the third stage use as vertical displacements: up, down, down, up, and down, up, up, down, as shown in Figure 1(d).

The sequence of piecewise linear functions thus constructed converges to a continuous function $f_z : [0,1] \longrightarrow R$ $(z < 1)$, which, by virtue of its definition, perfectly interpolates the original three data points. Figure 2 exhibits the limiting functions for varying values of z. As shown in Figure 2(a), when z equals zero, linear interpolation between the data points is obtained. As seen in Figures 2(b, c, and d), when z increases the resulting function becomes increasingly jagged. For $z \leq 0.5$, f_z may be shown to be differentiable almost everywhere (with respect to the Lebesgue measure). But, as z is increased beyond 0.5, f_z losses its differentiability and its graph covers more and more space on the plane leading to fractal (intermediate) dimensions, D, between 1 and 2, Barnsley (1986, 1988). The

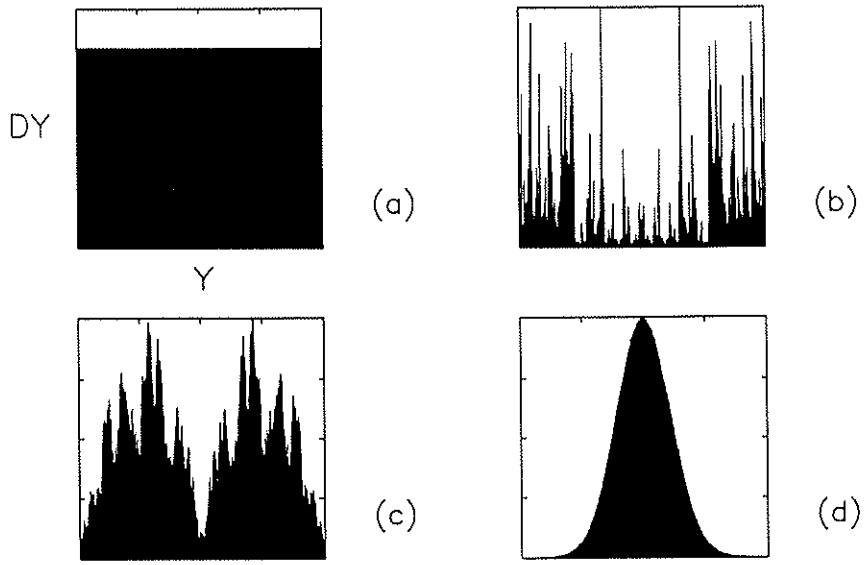

Figure 3: Derived Measures $Y = f_z(U)$ for the fractal interpolators in Figure 2

resulting graphs are in all cases *self-affine*: if f_z is restricted over any stage n subinterval $[(i-1)\cdot 2^{-(n+1)}, i\cdot 2^{-(n+1)}], i = 1, \ldots, 2^{n+1}$, and if such graph is adequately enlarged (with two distinct horizontal and vertical scales), then the whole function f_z over $[0, 1]$ is recovered. All functions f_z, even in the case when the fractal dimension of its graph is one, are examples of *deterministic fractal interpolating functions*, as introduced by Barnsley (1986, 1988).

As any function f_z is recursively constructed, two (probability) measures are naturally generated by counting the relative frequencies of the acquired points in the x and y coordinates. For the example in Figure 1, a uniform measure is obtained in x. This is easily seen because additional points at any stage are always in the middle of previous ones. In y, different measures appear depending on the parameter z, Puente (1992). Due to the continuity of the interpolating function, measures in y may be interpreted as being derived from the uniform measure in x via f_z, i.e. $Y = f_z(U)$, with U denoting the uniform probability measure in $[0, 1]$ and Y representing the derived measure (random variable) in y. Figure 3 shows the measures in y corresponding to the cases reported in Figure 2. As expected, when $z = 0$ a uniform measure is also obtained in y, Figure 3(a). As z is increased and as f_z becomes increasingly jagged, non-uniform derived measures of varying shapes are obtained, see Figures 3(b, c, and d). Notice that these graphs provide a (normalized) portrait of the number of crossings by the alternative functions f_z. As z approaches 1, the graph of f_z nearly fills-up the plane and has a fractal dimension arbitrary close to 2. As seen in Figure 3(d), the obtained derived measure closely resembles a Gaussian. That a limiting Gaussian is obtained in this case can be proven mathematically, Puente et al. (1996).

As mentioned in the introduction, multifractal measures are being increasingly identified

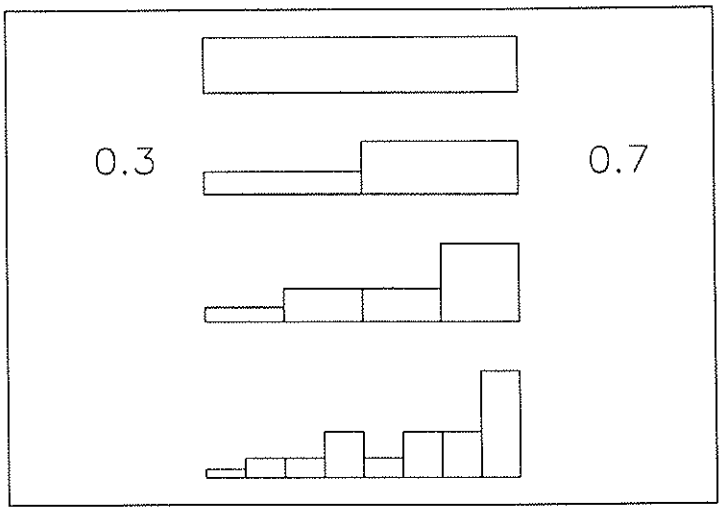

Figure 4: Recursive construction of binomial multifractal measure.

as relevant models of physical phenomena, especially in circumstances related to turbulence. Such measures also appear in the classical problem of the gambler's ruin in relation to the strategy of bold play, see for example Dubins and Savage (1968), Feller (1968), Billingsley (1983) and Feder (1988); and in the structure of the width function of Peano river networks, see Marani et al. (1991). They can be easily generated using a recursive procedure. Figure 4 illustrates the construction of a multiplicative binomial multifractal having equal length scales. An originally uniform bar is cut by a prespecified factor p, $0 < p < 1$, $p \neq 0.5$, say $p = 0.3$. Then, the first piece is stretched and the second piled-up so that a stair with two steps of equal lengths and masses p and $(1-p)$ is obtained. The process is repeated in each piece ad-infinitum. At stage n of the construction there are $\binom{n}{k}$ segments of length $(1/2)^n$ and mass $p^k \cdot (1-p)^{n-k}$, for $k = 0, 1, \ldots, n$, thus forming a "layered" measure. In the limit, when n tends to infinity, the number of layers also goes to infinity and the set of points that corresponds to each layer becomes a fractal subset of the interval $[0, 1]$ (like the classical Cantor set). For this reason the measure obtained, $M(p)$, is termed *multifractal*, see Mandelbrot (1989). Multiple-layered behavior has been observed in turbulence. In fact, the spacings between layers in fully-developed turbulence are very nicely fitted by those given by Figure 4 precisely when $p = 0.3$, Meneveau and Sreenivasan (1987). Binomial multifractals with different length scales are obtained if all mass redistributions are made over subintervals of unequal lengths. When the original mass is partitioned into more than two pieces, general *multiplicative multinomial multifractal measures* are obtained. It will be shown later that these measures appear in a very natural way when computing a fractal interpolator following a Monte Carlo approach.

If arbitrary binomial multifractals, like the one constructed in Figure 4 for any $0 < p < 1$, $p \neq 0.5$, replace the uniform distribution in x (i.e. when $p = 0.5$), then additional flexibility is gained in regards to derived patterns (distributions), see Puente (1992, 1994). Derived

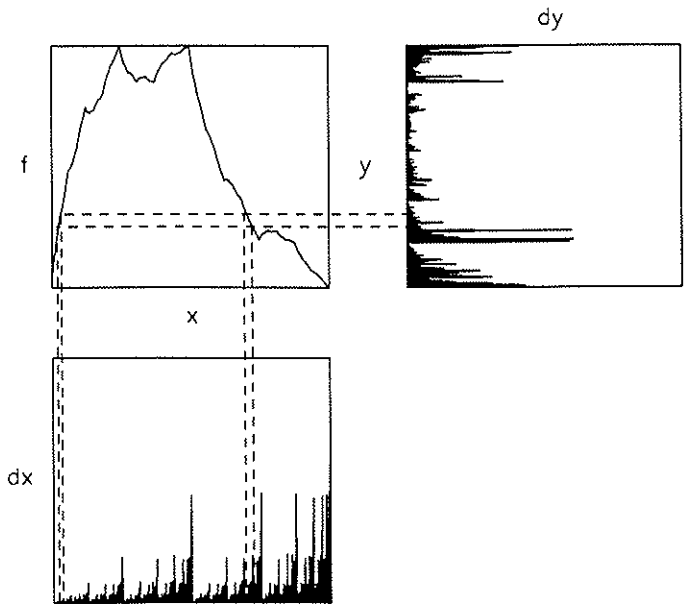

Figure 5: Construction of derived measures. $dy = f(dx)$.

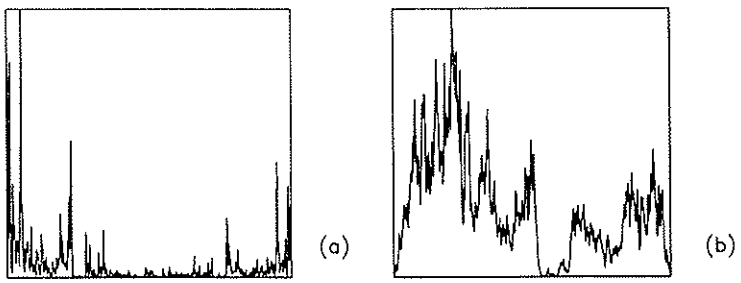

Figure 6: Examples of derived measures along a line: (a) exponential, (b) log-normal.

measures exhibit: (i) multifractal behavior (when z is small), (ii) absolutely continuous apparence (if z is large), and (iii) a Gaussian distribution (whose parameters depend on p) when z tends to 1.

Figure 5 illustrates the derived distributions construction for the most general case, see Benjamin and Cornell (1970). The measure in y, dy, (at y_0) is found by adding the corresponding "probabilities" in x, dx, (sum over all the x_0 with $f_z(x_0) = y_0$). Notice that the measure in y ($Y = f(X) = f_z(M(p))$) may be thought as a weighted projection of the function f_z, with the weights given by the measure $M(p)$. These derived measures possess a physical interpretation as they may be thought of as images or "projections" of turbulence.

Figure 6 shows a couple of derived measures along a line which illustrate the suitability of the *fractal-multifractal* representation to describe hydrologic (geophysical) information. They represent plausible realizations of phenomena either in time or in space, which have: (a) an exponential and (b) a log-normal distribution, respectively. Observe that without knowing their origin, both outcomes would have been qualified as "random". They give suitable data sets which are not self-similar nor self-affine and provide commonly observed marginal distributions in practice. In addition, the characterization of these patterns is quite parsimonious: both of these graphs were obtained interpolating the set of three data points employed in Figure 1, using $p = 0.3$.

It is important to stress at this time the main differences between the fractal-multifractal approach and classical statistical methods currently in use. First, the fractal-multifractal approach is entirely **deterministic**: both the parent multifractal measure and the transforming mapping may be uniquely obtained via simple recursive procedures. The data at hand is interpreted as a normalized distribution, a probability measure, which is encoded via a parent (deterministically generated) multifractal measure and a unique (and hence deterministic) fractal interpolating function. Second, instead of concentrating on the statistics of the actual realization or realizations at hand, the fractal-multifractal approach focuses on a wholistic description of geophysical patterns as we see them. Rather than using derived distributions to characterize the distribution of the data, the fractal-multifractal approach uses derived distributions to describe the data. It appears that the fractal-multifractal procedure, or others based on a similar idea, may provide a very parsimonious representation of natural data sets in time and in space.

2.2 Fractal Interpolation in Two Dimensions

The previous geometric construction may be carried mathematically and extended to any number of interpolating points in the plane. As explained in Barnsley (1988), the interpolating functions may be obtained as *attractors* of a set of contractile affine mappings. Specifically, given a set of $N+1$ data points on the plane, $\{(x_n, y_n), x_0 < x_1 < \cdots < x_N, n = 0, 1, \ldots, N\}$, and a set of N contractile affine maps of the form

$$w_n \begin{pmatrix} x \\ y \end{pmatrix} = \begin{pmatrix} a_n & 0 \\ c_n & d_n \end{pmatrix} \begin{pmatrix} x \\ y \end{pmatrix} + \begin{pmatrix} e_n \\ f_n \end{pmatrix}; \quad 0 \leq |d_n| < 1, \qquad n = 1, \ldots, N \qquad (1)$$

subject to

$$w_n \begin{pmatrix} x_0 \\ y_0 \end{pmatrix} = \begin{pmatrix} x_{n-1} \\ y_{n-1} \end{pmatrix}, \quad w_n \begin{pmatrix} x_N \\ y_N \end{pmatrix} = \begin{pmatrix} x_n \\ y_n \end{pmatrix}; \quad n = 1, \ldots, N, \tag{2}$$

an interpolating function f may be found such that $G = \cup_{n=1}^{N} w_n(G)$ with G being the graph of f, $G = \{(x,\ f(x)) | x \in [x_0,\ x_N]\}$. Barnsley (1986, 1988) showed that f exists, is continuous, is unique, and passes through each data point. Furthermore, (1) and (2) yield 4 equations in 5 unknowns for each $n \in \{1, \ldots, N\}$ enabling the solution of 4 parameters in terms of the remaining one and the data set. The vertical scalings d_n are typically chosen as the free variables. Once all parameters are fixed, it may be shown that the fractal dimension of G is $D = \max(1, D_0)$, where D_0 is the unique solution of

$$\sum_{n=1}^{N} |d_n| a_n^{D_0 - 1} = 1. \tag{3}$$

The geometric example in Figure 1 is recovered by setting $d_1 = -d_2 = z$. The graphs in Figure 6 are recovered by setting $d_1 = -d_2 = 0.45$ and $d_1 = d_2 = -0.70$, respectively.

The graph G can be constructed following simple deterministic recursive (geometric) rules (Barnsley 1988, Puente 1992). For instance, it may be found computing an infinite N-ary tree rooted at one of the data points. The first N nodes of such a tree are the images of the chosen data point, obtained using the affine mappings $w_1, \ldots, w_N$. The tree continues by applying the mappings to the newly acquired points on G, and so on. This corresponds to the procedure explained in Figure 1. Another simple way of creating the graph, G, is via a Monte-Carlo approach called the "chaos game" in which successive points are found recursively through images of (an arbitrary) data point employing the maps w_n according to a (fixed) set of weights p_n ($\sum_{n=1}^{N} p_n = 1, p_n > 0, n = 1, \ldots, N$). Instead of finding the whole N-ary tree, this method follows a single branch. This second procedure works due to an ergodic theorem (Barnsley, 1988) and it is a more convenient procedure for computer simulations. It must be stressed that this Monte-Carlo approach does not add any randomness to the final unique (and hence *deterministic*) outcome G.

By counting the number of times image points fall into a small interval in either the x or y axis, the methods above induce unique stationary measures in x and y, X and Y respectively (Barnsley 1986). As previously explained, the derived measures, which depend on the method of construction, can be scaled and thought of as probability distributions so that $Y = f(X)$ is the derived distribution of X via f. Given the structure of the first component of the affine mappings (see equation (1)), the unique measures in x induced by the chaos game are the deterministic multifractals with parameters p_n and length scales given by the data spacings, as explained on the previous section. As mentioned before, diverse measures appear in y depending on the nature of the affine mappings: they could be either non-smooth (i.e. multifractal as the parent measure in x) or absolutely continuous (as the fractal dimension D increases). In the limit, when the graph G of the fractal function fills up the plane (as $D \to 2$), the limiting derived distribution is Gaussian. This fact illustrates that there is a simple deterministic connection between intermittent (turbulent-based) measures and the harmonious Gaussian. The connection (via plane-filling fractal

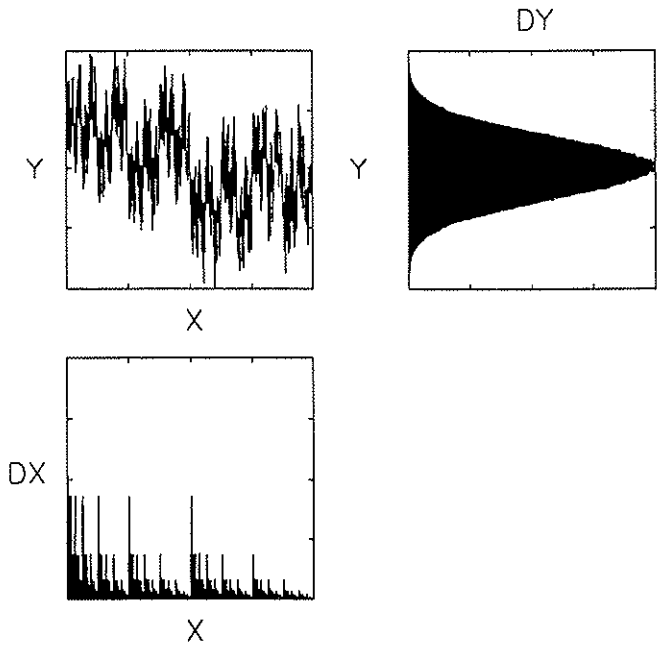

Figure 7: From turbulence to order, After Puente (1992).

functions) is particularly relevant because it ties up two very different behaviors observed in nature: irregularity and order, Puente (1992, 1994). Figure 7 illustrates this limiting case, for a binomial multifractal measure (DX) being transformed into a Gaussian distribution (DY). That this is the case (in the limit) may be proven mathematically, Puente et al. (1996).

When the fractal function is not plane-filling, the derived measures obtained can not be Gaussian. Instead, they are measures, as will be illustrated shortly, that resemble natural phenomena, like the rainfall patterns under study. The "fractal connection" does not lead to a Gaussian, but instead "bridges the gap" between turbulence (disorder) and other kinds of "disorder", as observed in natural patterns.

The derived measures in Figure 6 were obtained playing the chaos game employing a couple of affine transformations. As more affine functions are used, more flexibility is gained. For example, one may define three affine functions but only use two of them to arrive at Cantorian measures in x. This leads to derived distributions that may contain "holes". As seen in Figure 8, these objects may be of use in the modeling of phenomena such as rainfall which alternate between "active" and "dormant" states. Both graphs in Figure 8 interpolate $\{(0,0),\ (0.25,0.5),\ (0.5,1),\ (1,0)\}$. The first one is obtained when $d_1 = 0.6$, $d_2 = -0.2$, $d_3 = 0.2$ and $p_1 = 0.6$, $p_2 = 0$, $p_3 = 0.4$, while the second uses $d_1 = 0.5$, $d_2 = -0.4$, $d_3 = -0.4$ and $p_1 = 0.7$, $p_2 = 0$, $p_3 = 0.3$.

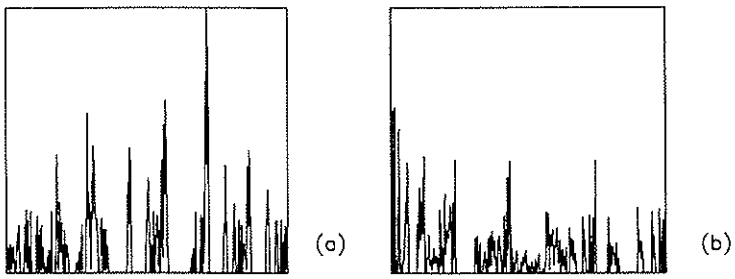

Figure 8: Examples of derived measures along a line based on Cantorian parents.

2.3 Fractal Interpolation in Three Dimensions

Analogous to the two-dimensional case, one may consider $N+1$ data points, $\{(x_n, y_n, z_n) : x_0 < \cdots < x_N; n = 0, 1, \ldots, N\}$, and a set of N contractile maps of the form

$$w_n \begin{pmatrix} x \\ y \\ z \end{pmatrix} = \begin{pmatrix} a_n & 0 & 0 \\ c_n & d_n & h_n \\ k_n & l_n & m_n \end{pmatrix} \begin{pmatrix} x \\ y \\ z \end{pmatrix} + \begin{pmatrix} e_n \\ f_n \\ g_n \end{pmatrix}, n = 1, \ldots, N \tag{4}$$

such that

$$A_n = \begin{pmatrix} d_n & h_n \\ l_n & m_n \end{pmatrix} \tag{5}$$

has L_2-norm less than 1 ($\|A_n\|_2 = \sqrt{\lambda_{\max}(A_n^T A_n)} < 1$) and

$$w_n \begin{pmatrix} x_0 \\ y_0 \\ z_0 \end{pmatrix} = \begin{pmatrix} x_{n-1} \\ y_{n-1} \\ z_{n-1} \end{pmatrix}, \quad w_n \begin{pmatrix} x_N \\ y_N \\ z_N \end{pmatrix} = \begin{pmatrix} x_n \\ y_n \\ z_n \end{pmatrix}; \quad n = 1, \ldots, N. \tag{6}$$

Now, a three-dimensional "wire" $G = w_1(G) \cup \ldots \cup w_N(G)$ appears, which is the unique attractor of the mappings $\{w_1, \ldots, w_N\}$, and the graph of a continuous deterministic function from $[x_0,\ x_N]$ to the yz-plane. The construction leaves now four free parameters per map, with a_n, c_n, e_n, f_n, g_n, and k_n all determined in terms of d_n, h_n, l_n, m_n and the $N+1$ data points. Transforming to polar coordinates, redefine the submatrix A_n

$$A_n = \begin{pmatrix} d_n & h_n \\ l_n & m_n \end{pmatrix} = \begin{pmatrix} r_n^{(1)} \cos\theta_n^{(1)} & -r_n^{(2)} \sin\theta_n^{(2)} \\ r_n^{(1)} \sin\theta_n^{(1)} & r_n^{(2)} \cos\theta_n^{(2)} \end{pmatrix} \tag{7}$$

The entries on these matrices and the interpolating data points constitute the parameter set Θ which completely characterize an interpolating function f.

If the magnitude of the scaling parameters $r_n^{(i)}$ are all less than one, then there is a unique attracting set G with the desired properties, Barnsley (1988). Moreover, the attractor G

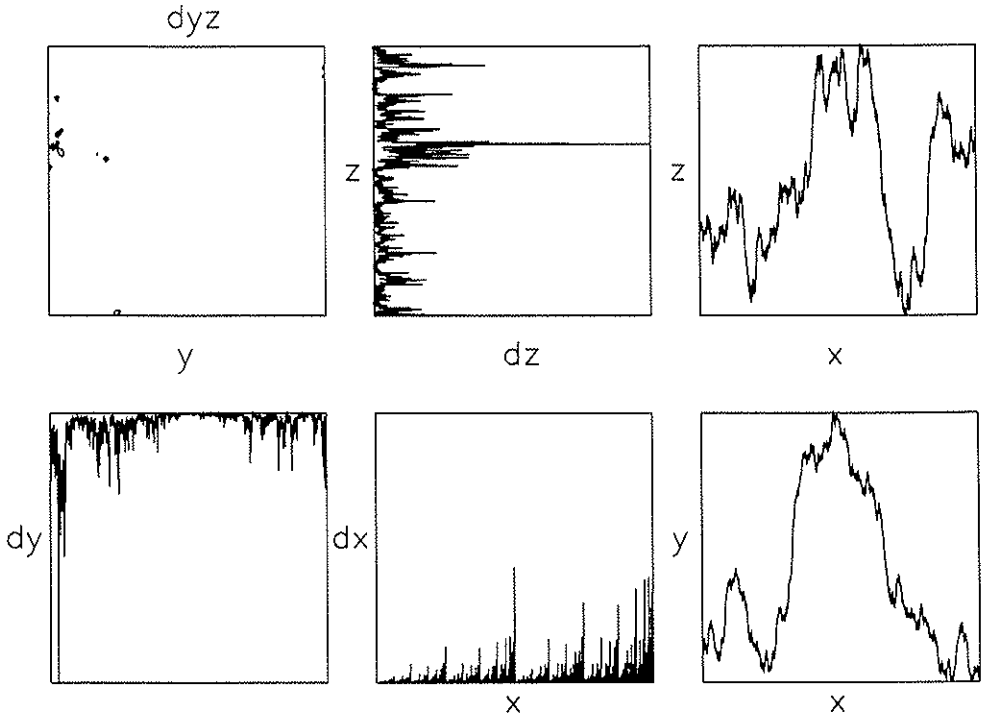

Figure 9: Three-dimensional fractal interpolator projections and derived measures. $\{(0, 0.1, 0), (0.5, 1, 0.4), (1, 0, 0.2)\}$. $r_1^{(1)} = r_1^{(2)} = -0.6$, $\theta_1^{(1)} = \theta_1^{(2)} = 45$, $r_2^{(1)} = 0.6$, $r_2^{(2)} = -0.6$, $\theta_2^{(1)} = \theta_2^{(2)} = 45$, $p_1 = 0.3$, $p_2 = 0.7$ (angles in degrees).

becomes fractal as the magnitude of the scaling parameters increases towards one (Barnsley 1988). Analogous to the two-dimensional case, a formula may be derived for the fractal dimension of G, Puente and Klebanoff (1994).

Figure 9 shows the analogous to Figure 5 for the three-dimensional case. In addition to a parent measure in x, a fractal interpolating function from x to y, and a derived measure in y, now there are also an interpolating function from x to z (a projection of the unique "wire" in the $x - z$ plane), a derived measure in z and more importantly a joint derived measure in yz. As may be seen, phenomena along y and z may be correlated and, as before, need not to be strictly self-similar or self-affine. Rainfall in time may be modeled by considering the wire projection either in $x - y$ or in $x - z$. Now there are "hidden" relationships being used which could account for variables such as reflectivities, water content, temperature, etc. As will be illustrated later, the projections over the $y - z$ plane may be employed to model spatial rainfall.

As in the two-dimensional case, in the limit when the r_n's tend to 1 one obtains joint bivariate Gaussian distributions, Puente and Klebanoff (1994). By varying the parameter set Θ one may obtain alternative cross-correlations which are geometrically explained in terms of the xy and xz projections of the corresponding unique function $f = f_\Theta$. When a Cantorian measure is used in x still a space-filling fractal leads to a bivariate Gaussian in

yz. As in two-dimensions, a Cantorian measure in x leads to increased freedom in derived measures over the plane when the function f is away from being space-filling.

It is not hard to generalize the procedures given here so that derived measures are defined over $\mathcal{R}^m$, and in particular over $\mathcal{R}^3$.

2.4 Statistics of Multifractals

Consider a measure μ over a one-dimensional domain of size L, defined up to some minimum scale δ_τ. To describe it, divide it into N pieces of size $\delta = L/N \geq \delta_\tau$, and call $\mu_i(\delta)$ the measure in the ith piece, $1 \leq i \leq N$.

The Lipschitz-Hölder exponents α quantify the strenght of the measure's singularities. Typically, they are location dependent and are found from the scaling relation, $(\delta \to 0)$:

$$\mu_i(\delta) \sim \delta^\alpha. \tag{8}$$

Let $N(\alpha, \delta)$ be the number of pieces for a given resolution δ where a given value of α is found, and define $f(\alpha)$ from the scaling relation:

$$N(\alpha, \delta) \sim \delta^{-f(\alpha)}. \tag{9}$$

Then, $f(\alpha)$ may be thought of as the fractal dimension of the set of points that corresponds to a singularity α, and a graph of α vs. $f(\alpha)$ is called the *multifractal spectrum* of the measure.

Loosely speaking, a measure is *multifractal* when its multifractal spectrum exists and has the shape of an inverted parabola. $f(\alpha)$ can not be negative for a single measure. This is because an observed value of α in yields for $N(\alpha, \delta)$ at least a value of 1, and hence an exponent of at least 0 for $f(\alpha)$. The maximum value of $f(\alpha)$ corresponds to the fractal dimension of the measure's support. This value equals 1 in case of a measure defined over an interval.

A generally equivalent way to arrive at multifractals is obtained by considering the scaling laws of the moments of the measure. This involves

$$\sum_{i=1}^{N} [\mu_i(\delta)]^q \sim \delta^{-\tau(q)} \ , \tag{10}$$

where $\tau(q)$ is the measure's qth *mass exponent.* As q is varied, the different orders of magnitude within the measure are probed. For instance, when q is large and positive, the sum is dominated by large $\mu(\delta)$'s; while if q is negative, the sum is dominated by small $\mu(\delta)$'s. Loosely speaking again, a measure is multifractal when $\tau(q)$ is a non-linear convex function. The measure's *generalized dimensions* are defined in terms of the mass exponents by $D(q) = \frac{\tau(q)}{1-q}$, Hentschel and Procaccia (1983). $D(0)$ is the fractal dimension of the support of the measure, $D(1)$ is the entropy dimension, and $D(2)$ is the correlation dimension. For an absolutely continuous measure over the line (i.e. uniform, Gaussian, etc.) the mass exponents become the straight line $\tau(q) = 1 - q$, and then all generalized dimensions are equal. These measures are clearly not multifractals.

When $f(\alpha)$ and $D(q)$ are smooth functions of α and q, the following heuristic argument can be made, Halsey et al. (1986):

$$\sum_i [\mu_i(\delta)]^q \sim \sum_\alpha \delta^{\alpha q} \delta^{-f(\alpha)} \sim \delta^{min\{\alpha q - f(\alpha)\}}. \tag{11}$$

This implies Legendre relationships between $\tau(q)$ and $f(\alpha)$:

$$\alpha = -\frac{d\tau}{dq}, \tag{12}$$

$$f(\alpha) = \alpha\, q + \tau(q). \tag{13}$$

Even though these Legendre relations are valid for many typical multifractal models (e.g. multinomial multifractals and measures arising from stochastic cascades with strongly bounded generators, Holley and Waymire (1992), there are examples in which they do not hold (e.g. Holley and Waymire, 1992).

Yet another way for arriving at the concept of multifractality has been developed by Schertzer and Lovejoy (1987). Instead of working with the measure $\mu(\delta)$, attention is centered on the extremes of the density $\epsilon_\lambda = \mu(\delta)/\delta$. This leads to the *codimension function* of the data, $c(\gamma)$, via the scaling relation:

$$Prob[\epsilon_\lambda \geq \lambda^\gamma] \sim \lambda^{-c(\gamma)}. \tag{14}$$

The multifractal spectrum and the codimension function contain precisely the same information when low values of α are considered ($q > 0$). In fact, for one-dimensional continuous data sets the codimension function is simply related to the left side of the multifractal spectrum via the relations: $\gamma = 1 - \alpha$ and $c(\gamma) = 1 - f(\alpha)$. For data sets defined over two or three dimensions the codimension is preferred because it does not depend explicitly on the dimension being studied, Schertzer and Lovejoy (1989).

Several procedures have been proposed in the literature to estimate the multifractal spectrum (or codimension function) of a measure. Following the "mass exponents" technique, the $\tau(q)$'s are found first (via simple regressions using its definition) and then the Legendre relations are used to get $f(\alpha)$.

It is possible to get the multifractal spectrum directly without Legendre transforms, Chhabra and Jensen (1989). The "direct method" requires usage of normalized measure

$$\zeta_i(q,\delta) = \frac{\mu_i(\delta)^q}{\sum_j \mu_j(\delta)^q}\ , \tag{15}$$

such that an "average" α and the corresponding $f(\alpha)$ are

$$\alpha(q) = \lim_{\delta \to 0} \frac{\sum_i \zeta_i(q,\delta) log(\mu_i(\delta))}{log\delta}\ , \tag{16}$$

and

$$f(q) = \lim_{\delta \to 0} \frac{\sum_i \zeta_i(q,\delta) log(\zeta_i(q,\delta))}{log\delta}. \tag{17}$$

This procedure, based on information theoretic ideas, avoids employing Legendre transforms but results in a spectrum that satisfies them. Practical use of this method in fully developed turbulence has been reported by Chhabra et al. (1989).

The codimension function may also be obtained following several approaches. These include the Probabilistic Distribution Multiple Scaling (PDMS) technique, and the Double Trace Moment procedure of Lavallée et al. (1991). We shall concentrate only on the methods for multifractal spectrum in lieu of the existing equivalences between $f(\alpha)$ and $c(\gamma)$.

3 Results and Their Significance

This section contains the analysis made on several uses of the fractal-multifractal methodology. They include the following specific applications: (i) representation of high resolution temporal rainfall records, (ii) determination of chaos and stochasticity of generated series, and (iii) potential of the geometric methodology in dealing with space-time rainfall.

3.1 Description of High Resolution Rainfall

The suitability of the fractal-multifractal approach for representing real rainfall records is illustrated in this section. For this purpose, three high resolution storms were used: one in Boston previously analyzed by Rodriguez-Iturbe et al. (1989), and two in Iowa City gathered and analyzed by Georgakakos et al. (1994). Table 1 provides relevant information about these events.

Table 1: Information for high resolution storms.

Storm	Location	Date	Sampling Time (sec)	Data Points	Duration (hours)
Boston	Boston	10/25/80	15	1990	8.3
Iowa2	Iowa City	11/01/90	5	8192	11.4
Iowa3	Iowa City	11/30/90	5	8192	11.4

The parameters that need to be specified for a fractal-multifractal description of a given data set are: (a) the points by which the fractal interpolation function passes (*localization parameters*); (b) the sequences of ups and downs and their magnitude (*regularity parameters*, z's), and (c) the quantities that dictate how to recursively construct the multifractal measure (*intermittency parameters*, p's). As noticed from the construction of the components of the fractal-multifractal representation, i.e. Figure 5, the shape of the derived measure dy varies *continuously* on all the surrogate geometric parameters. This property implies that a small change in localization, regularity or intermittency parameters leads to a small outcome change, e.g. a nearby and *different* derived measure dy.

Although it appears that alternative derived measures are found by varying the surrogate parameters, unfortunately there is neither a simple analytical formula that gives the derived

measure dy, nor its most common statistics, in terms of these parameters. This implies that the inverse problem for a given data set can not be obtained analytically, but will require complete calculations via chaos game simulations. Fortunately, these calculations are not extensive and a numerical approach can be implemented. At the end, the inverse problem becomes complicated due to: (i) the large number of combinations of surrogate parameters (even with few interpolating points), and (ii) the practically infinite number of derived measures that may be generated, many having common features among themselves. It has been our experience that a cataloguing exercise is a must before attempting any sophisticated search algorithm.

Besides looking at pages on an interactive catalogue, the fractal geometric parameters for the three storms reported in this work were obtained using multidimensional optimization procedures. These algorithms minimized squared differences between real and fractal-multifractal outcomes in terms of a combination of classical statistical indicators and multifractal characteristics. The statistical qualifiers included moments of the data sets in both the time and intensity axis, and the autocorrelation function (power spectrum) of the records. The multifractal characteristics considered accounted for the mass exponents function $\tau(q)$ for the data sets, i.e. equation (10).

Given the complex nature of the data sets to be fitted, a two-step optimization procedure was considered. During the first stage, a preliminary set of parameters was found employing the *multidimensional simplex* method (Press et al., 1989), starting the procedure using parameter values obtained via the cataloguing exercise. On the second stage, those parameters became initial conditions for more sophisticated searching procedures. The methods of *simulated annealing* (Otten et al., 1989) and/or sequential *quadratic programming* (Zhou and Tits, 1993) were used at this stage. It is worth reemphasizing that despite the success attained by the procedures, heuristic knowledge on behalf of the user is key in order to search for improved solutions.

Tables 2, 3 and 4 provide relevant statistical information for the observed and predicted data sets on the three storms of Table 1. These statistics include:

- central moments for the records seen from the time axis, $M(y)$,
- moments around the mode for records seen from the time axis, $M(y)^*$,
- central moments computed from the rainfall intensity axis, $M(dy)$
- time lag where first minimum of autocorrelation function happens, $\tau(flm)$,
- the scaling exponent α for the power spectrum, i.e. $S(\omega) \sim \omega^{-\alpha}$,
- mass exponents for the indicated weights q, $\tau(q)$, and
- the information dimension for the data, $D(1)$.

The mass exponents above were computed fitting the best regression on equation 10 using four consecutive resolutions. The reported values of the information dimension were found employing the method of mass exponents taking four regression points, i.e. the Legendre transforms on equations 12 and 13.

Table 2: Relevant statistics for high resolution Boston storm.

Moment	Order	Real value	Predicted value	Error (%)
$M(y)$	1	0.445	0.439	1
	2	0.237	0.215	9
	3	0.265	0.211	20
	4	2.502	2.412	4
$M(y)^*$	1	0.547	0.535	2
	2	0.258	0.235	9
	3	-0.854	-0.925	8
	4	2.272	2.273	0
$M(dy)$	1	0.075	0.077	3
	2	0.074	0.072	3
	3	3.643	3.179	13
	4	28.76	24.84	14
$\tau(flm)$		23	16	30
α		2.711	2.686	1
$\tau(q)$	-1.0	2.034	2.139	5
	-0.2	1.204	1.202	0
	0.6	0.396	0.396	0
	1.4	-0.391	-0.392	0
	2.2	-1.161	-1.153	1
	3.0	-1.908	-1.873	2
	3.8	-2.629	-2.545	3
	4.6	-3.330	-3.184	4
	5.4	-4.014	-3.803	5
	6.2	-4.688	-4.411	6
$D(1)$		0.982	0.984	0

Table 3: Relevant statistics for high resolution storm Iowa2 in Iowa City.

Moment	Order	Real value	Predicted value	Error (%)
$M(y)$	1	0.382	0.407	7
	2	0.243	0.230	5
	3	0.702	0.605	14
	4	2.913	2.959	2
$M(y)^*$	1	0.413	0.419	1
	2	0.245	0.230	6
	3	0.313	0.458	46
	4	2.571	2.843	11
$M(dy)$	1	0.023	0.022	4
	2	0.050	0.048	4
	3	9.267	8.855	4
	4	115.8	120.5	4
$\tau(flm)$		6	8	33
α		1.300	1.351	4
$\tau(q)$	-1.0	1.881	2.043	9
	-0.2	1.195	1.208	1
	0.6	0.396	0.389	2
	1.4	-0.391	-0.374	4
	2.2	-1.166	-1.079	7
	3.0	-1.928	-1.749	9
	3.8	-2.677	-2.408	10
	4.6	-3.413	-3.062	10
	5.4	-4.138	-3.714	10
	6.2	-4.852	-4.364	10
$D(1)$		0.982	0.953	3

Table 4: Relevant statistics for high resolution storm Iowa3 in Iowa City.

Moment	Order	Real value	Predicted value	Error (%)
$M(y)$	1	0.480	0.476	1
	2	0.227	0.222	2
	3	-0.453	-0.563	24
	4	2.275	2.404	6
$M(y)^*$	1	0.664	0.652	2
	2	0.292	0.283	3
	3	-1.602	-1.655	3
	4	2.959	3.152	7
$M(dy)$	1	0.035	0.032	9
	2	0.062	0.060	3
	3	5.485	5.188	5
	4	51.00	43.55	15
$\tau(flm)$		7	28	300
α		1.480	1.268	14
$\tau(q)$	-1.0	1.986	1.829	8
	-0.2	1.200	1.198	0
	0.6	0.390	0.391	0
	1.4	-0.380	-0.381	0
	2.2	-1.113	-1.123	1
	3.0	-1.820	-1.841	1
	3.8	-2.514	-2.539	2
	4.6	-3.202	-3.219	1
	5.4	-3.888	-3.884	0
	6.2	-4.572	-4.537	1
$D(1)$		0.960	0.963	0

As may be seen, the fractal-multifractal description matches well the characteristics of the three storms considered.

The storm in Boston, which has the shortest of all data sets considered, has a large isolated maximum and several intermediate peaks, Figure 15. As may be seen in Table 2, excellent agreement is found for all the moments computed, with modal moments on the time axis ($M(y)^*$) being better that those found around the mean. As observed on such table, the magnitede of the time delay on the autocorrelation function where the first local minimum happens is preserved but the actual values do not match (23 vs. 16). This happens despite close agreement on power spectrum scaling, as evidenced by exponents α (computed for frequencies greater than 0.4) which differ by only 1%. The mass exponents for the storm in Boston are nicely reproduced, with errors that are less than 3% for q values between -0.2 and 3.8. Notice that these small errors translate into a precise fit of the information dimension $D(1)$. The results given in Table 2 were found employing a parameterization based on five interpolating points.

Table 3 contains the statistics for an Iowa City storm (Iowa2) and its corresponding fractal-multifractal fit based on three interpolating points. This storm contains a large localized peak and long periods (before and after the peak) of relatively little activity. As the central and modal moments on Table 3 reveal, the fractal-multifractal approach does preserve the location of the large peak and gives a representation which is very faithful in relation to the moments. The reproduction of the short time delay to the first minimum on the autocorrelation function of the real data (6 vs. 8), and the close agreement on the power-law power spectrum (1.3 vs. 1.35, for regressions using frequencies greater than 0.2) confirm the quality of the fractal-multifractal representation. It may be seen however, by comparing the Tables 2, 3 and 4, that this storm is the hardest one to fit in relation to multifractal characteristics. As may be seen in Table 3, the errors on the mass exponents function increase rapidly as $|q|$ increases. This leads to a fractal-multifractal prediction which has an "emptier" domain than the real data, i.e. the correlation dimension for the predictions is farther away from 1 than this attribute found for the real data.

The statistics for the other storm in Iowa City (Iowa3) are included in Table 4. This high resolution storm exhibits two large zones of peak activity, several medium-sized peaks, and a long zone of little "noisy" behavior, see the right hand portion of Figure 10. For this storm, a fractal-multifractal representation based on five interpolating points was employed. As may be seen by looking at Table 4, this storm in Iowa City is nicely captured, both in relation to its moments and also in regards to its multifractal characteristics.

Figure 10, for the storm Iowa3, illustrates that the fits obtained are not only statistical correct but also visually appealing, Puente and Obregón (1995). This graph shows the parent multifractal measure, the fractal interpolating function (from five interpolating points), and the deterministic description obtained for the records. The data set itself is displayed on the right hand side of the figure for comparison purposes. As may be observed, the location and magnitude of the peaks are well represented and the overall behavior ("noise") of both graphs is similar. Observe that the parent multifractal and fractal interpolating function combination are not trivial ones, but these two *deterministic* objects blend together to give a close representation of the observed records. That such a representation is possible suggests

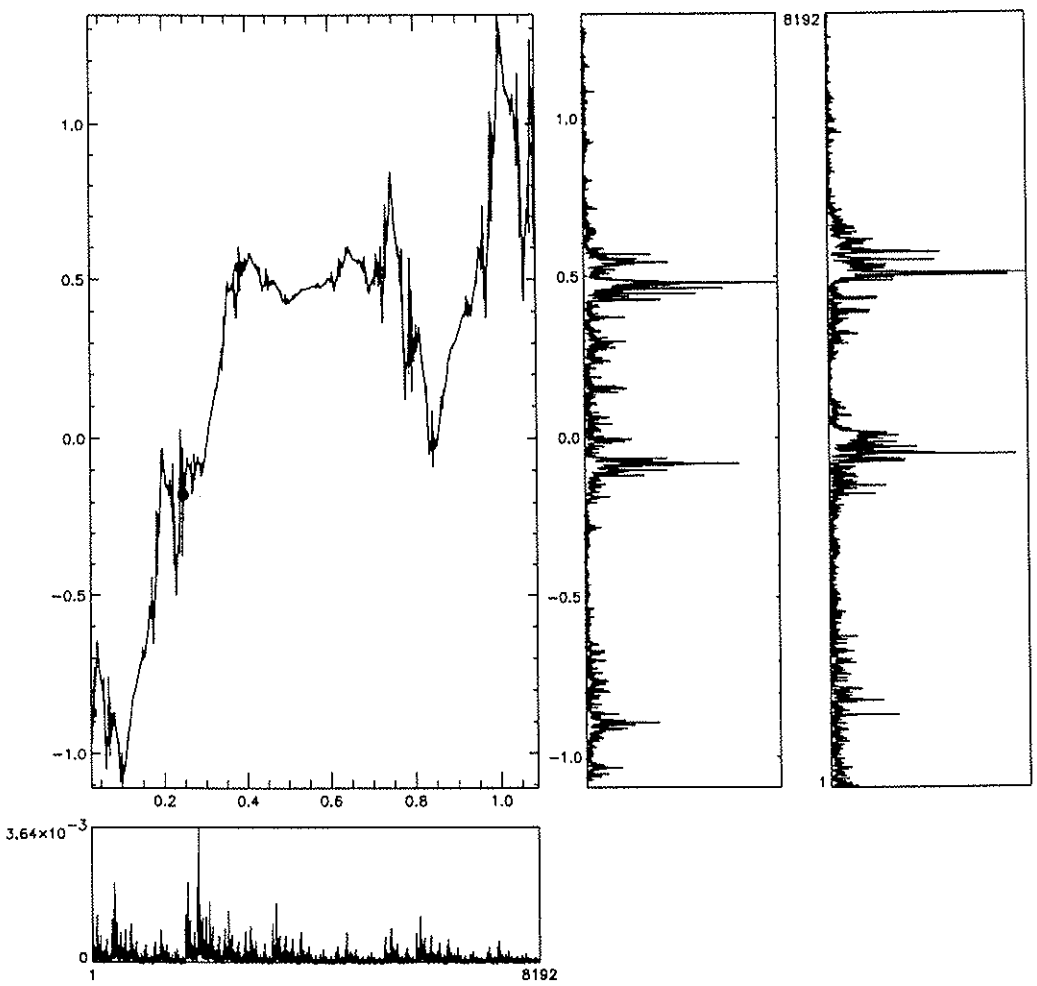

Figure 10: Predicted and real rainfall records for the Iowa3 storm in Iowa City. Fractal multifractal parameters: (a) localization, {(0.03, -0.87), (0.24, -0.17), (0.39, 0.54), (0.72, 0.52), (1.09, 0.92)}, (b) regularity, -0.53, -0.20, -0.13, -0.85, (c) intermittency: 0.25, 0.28, 0.25, 0.22.

indeed that actual records may be thought of as "weighted projections" without the need of stochastic descriptions.

Figures 11, 12 and 13 complement the statistical description given in Table 4. Figures 11 and 12 include the whole autocorrelation function ($\rho(\tau)$), power spectrum ($S(\omega)$) and the -5/3 line, data histogram ($f(dy)$), and multifractal spectrum ($f(\alpha)$) for the observed and approximated records, respectively. Notice the close agreement in:

(i) the exhibited power-law power spectrum, i.e. close α's as shown in Table 4 for $\omega > 0.1$,

(ii) the shape of the autocorrelation function, which includes the delay τ for which $\rho(\tau)$ equals e^{-1}, $(\tau(e-1))$, and the time delay to the first local minimum, $(\tau(flm))$,

(iii) the histogram of the records, which includes moments on the two axis $M(y)$ and $M(dy)$, and

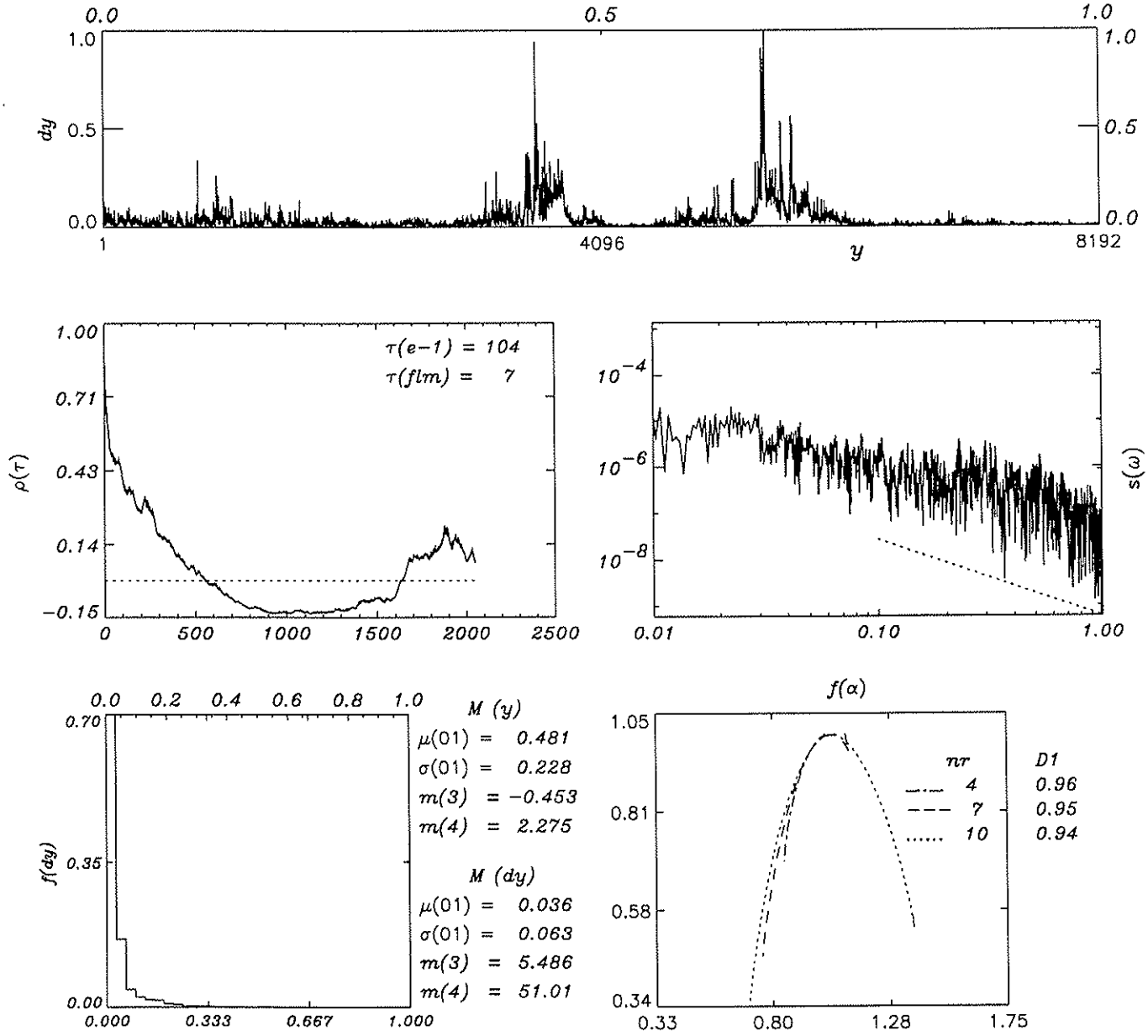

Figure 11: Statistics for observed Iowa3 storm in Iowa City: autocorrelation ($\rho(\tau)$), power spectrum ($S(\omega)$), data histogram ($f(dy)$), and multifractal spectrum ($f(\alpha)$).

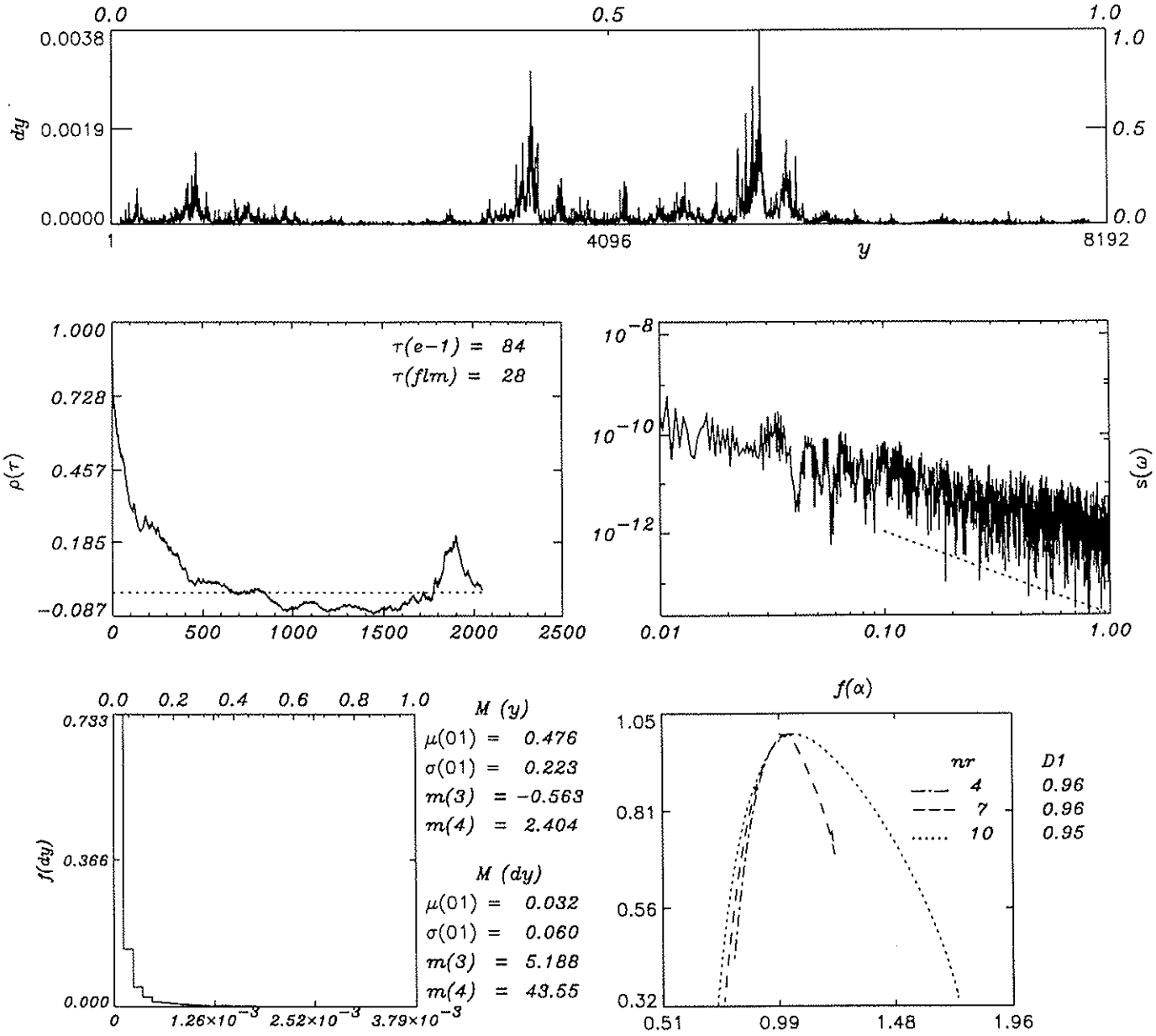

Figure 12: Statistics for predicted Iowa3 storm in Iowa City: autocorrelation ($\rho(\tau)$), power spectrum ($S(\omega)$), data histogram ($f(dy)$), and multifractal spectrum ($f(\alpha)$).

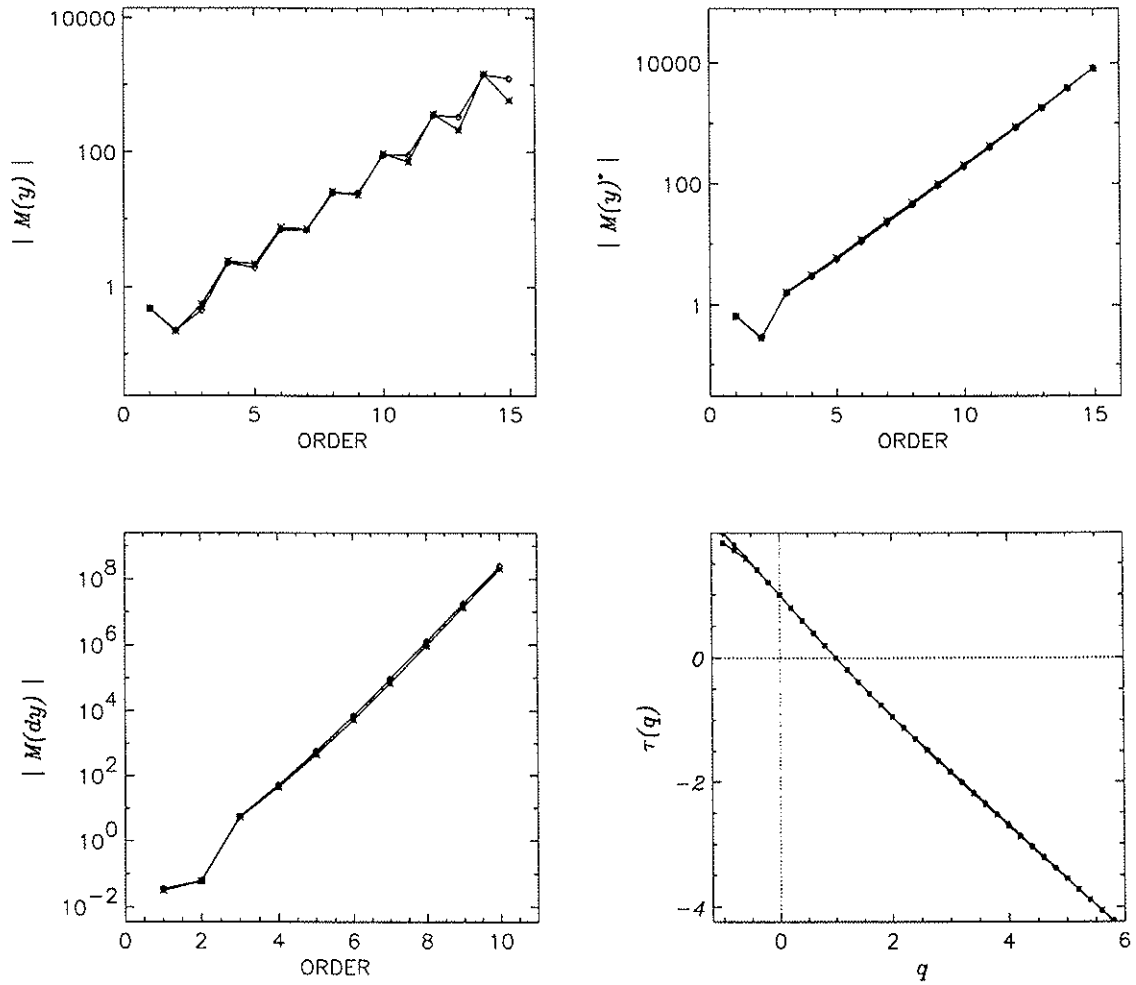

Figure 13: Moments for observed and predicted (*–*) Iowa3 storm in Iowa City: central moments in time ($M(y)$), modal moments in time ($M(y)^*$), central moments in intensity axis ($M(dy)$), and mass exponents ($\tau(q)$).

(iv) the left hand portion of the multifractal spectrum computed from the method of mass exponents, as exemplified by very close entropy dimensions ($D1$) calculated using a varying number of resolutions (nr).

Of course, the fractal-multifractal representation obtained for Iowa3 is not perfect. Clearly, it would be nice to have an even closer agreement on the details of the autocorrelation function of the data. That the simulated series preserve the moments of the actual data is further illustrated in Figure 13. This graph extends the results provided in Table 4. It includes the first 15 central and modal moments in the time axis (in semi-log scale), the first 10 central moments in the intensity axis (in semi-log scale), and the mass exponents function (found from $nr = 4$ regression points) for values of q between -1 and 6 and having as increment a value of 0.2. As may be seen, the agreement in regards to these attributes is excellent for Iowa3. It is worth mentioning that the calculated multifractal spectrum from the direct method (i.e. equations 16 and 17) gave the same results as the mass exponents method did.

Visual and statistical similarities (including multifractal behavior) have also been found for the other storms. This will be illustrated for the storm in Boston in the next section.

In addition to fractal interpolating functions in two dimensions, "hidden" variable rainfall descriptions, i.e. from equation 4 have also been computed. These projections of three-dimensional wires also result in close and suitable representations of available records. The suitability of such a representation is illustrated in Figure 14, which includes the actual Boston records on the third spot from the top. Observe that the other "storms" have features which are very similar to those of the Boston data, but their largest peaks occur at different times. Table 5 includes the variable surrogate parameters for the five "storms" in Figure 14. All these data sets have 3 interpolating points in three dimensions and share: $x_0 = 0$, $x_1 = 0.5$, $x_2 = 1$, $r_1^{(1)} = r_1^{(2)} = -0.6$, $\theta_1^{(1)} = \theta_1^{(2)} = 45$, $r_2^{(1)} = 0.6$, $r_2^{(2)} = -0.6$, $\theta_2^{(1)} = \theta_2^{(2)} = 45$, $p_1 = 0.3$, $p_2 = 0.7$. A pictorial representation of the building blocks of the second graph from the top in Figure 14 was already given in Figure 9. In fact, the second "storm" corresponds to the measure dz in Figure 9 (be aware of proper orientation).

It is important to emphasize that all records in Figure 14 have a large maximum, few intermediate spikes, and a rainfall variability which will be typically qualified as "noise". Observe that the fractal-multifractal representation results in measures which resemble the details present on actual records at a wide range of scales. A complete statistical analysis reveals that the representations given in Figure 14 do share similar statistical and chaotic characteristics. In fact, these series may be modeled as deterministic chaotic systems with few degrees of freedom, as found for the original data by Rodriguez-Iturbe et al. (1989). Details of a chaotic analysis of data sets similar to the ones shown in Figure 14 are given in the next section.

3.2 Chaos vs. Stochasticity in Temporal Rainfall

As briefly explained on the previous section, whether rainfall may be viewed as a deterministic chaotic process has attracted attention in the literature, i.e. Rodriguez-Iturbe et al. (1989). Given that it is possible to model complicated data sets by means of the fractal-multifractal representation, it is relevant to ask if the outcomes of the deterministic procedure

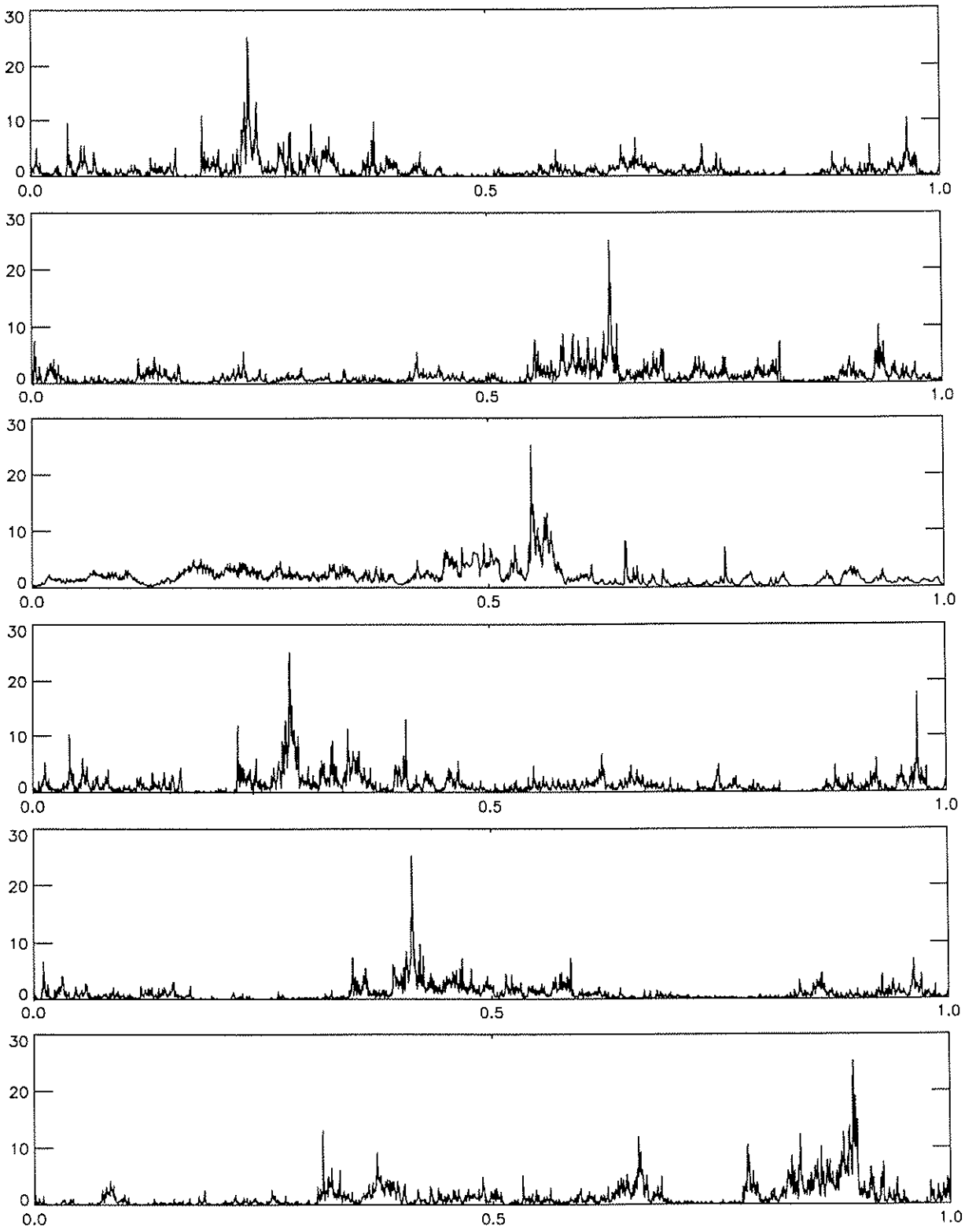

Figure 14: Hidden variable projections and a storm in Boston.

Table 5: Relevant surrogate parameters for "storms" in Figure 14.

Storm number (from the top)	Geometry					
	y_0	y_1	y_2	z_0	z_1	z_2
1	0.00	1.00	0.00	0.00	0.90	-0.20
2	0.10	1.00	0.00	0.00	0.40	0.20
4	0.00	1.00	0.00	0.00	1.00	0.00
5	0.10	1.00	0.00	0.00	0.50	0.00
6	0.10	1.00	0.00	0.00	0.20	0.40

lead to deterministic chaos. This section studies this question by: (i) using a suitable representation of the storm in Boston, and (ii) considering a host of projections from alternative wires in two-dimensions. Before giving such results, a brief review of chaos theory and related techniques is provided.

3.2.1 A Brief Review of Chaos Theory

The possibility that natural and apparently random time series (i.e. with broad band spectrum) may be described by sets of few ordinary differential equations, which exhibit chaotic behavior, has attracted considerable interest in the literature. Clearly, the physical description of a phenomena can be greatly simplified if a small number of modes dominates the dynamics. One of the aims of nonlinear analysis of time series is the discrimination of behavior between low-dimensional chaos and high-dimensional "random" behavior.

Key in the definition of chaotic behavior is the proper identification of low-dimensional strange attractors. Phase-space reconstruction is typically made by time embeddings of the records $X(t)$, i.e. vector time series of increasing dimensions N:

$$\mathbf{X}(t_i) = \{X(t_i),\ X(t_i+\tau),\ \ldots,\ X(t_i+(N-1)\tau\}, \tag{18}$$

with an appropriate delay τ. Stable fractal dimension of the obtained cloud of dots, after a certain dimension N_0, is recognized as a precursor of chaotic behavior. Once the embedding dimension N_0 is found, a positive value for the largest Lyapunov exponent of the system confirms the chaotic nature of the data.

Accurate definition of the delay τ is crucial for the proper reconstruction of strange attractors, and several suggestions have been made in the literature, e.g. Albano et al. (1988, 1991), Fraser and Swinney (1986), Fraser (1989). For this report τ was defined as the delay time to the first local minimum of the autocorrelation function of the data being considered.

The proper determination of N_0 is typically made employing the correlation dimension and Kolmogorov entropy, Grassberger and Procaccia (1983a, b). For the correlation function

at a given embedding N one defines

$$C_N(\epsilon) = \frac{1}{M^2 - M} \sum_{i \neq j}^{M} H\left(\epsilon - \|\mathbf{X}(t_i) - \mathbf{X}(t_j)\|\right), \tag{19}$$

where H is the Heaviside step function, M is the number of points in the vector time series $\mathbf{X}(t_i)$ and the vertical bars indicate the norm of the vector.

If an attractor for the system exists then the *correlation dimension*, $D(2)$, for the system satisfies

$$C_N(\epsilon) \sim \epsilon_N^{\nu} \tag{20}$$

and

$$\nu_N \sim \nu = D(2) \tag{21}$$

when $\epsilon \to 0$ and $N \to \infty$. Stabilization of $D(2)$ for a small value of N_0 gives rise to possible chaotic behavior because the correlation dimension approximates the fractal dimension of the strange attractor.

Efficient algorithms for correlation dimension are needed when data sets are large, specially when considering a large number of embedding dimensions. A typical procedure divides the phase-space into blocks and computes $C_N(r)$ for all points within the same block and only for some points that belong to different blocks, e.g. Grassberger (1990).

Another criteria for identifying strange attractors is the stabilization of the K_2 entropy of the flow, a lower bound of the Kolmogorov-Sinai entropy, e.g. Provenzale et al. (1991). K_2 is defined from successive correlation functions as follows:

$$log\left(\frac{C_N(\epsilon)}{C_{N+1}(\epsilon)}\right) \sim K_2(N) \tag{22}$$

and

$$K_2(N) \sim K_2 \tag{23}$$

for $\epsilon \to 0$ and $N \to \infty$. K_2 is thought to have the same qualitative behavior of the Kolmogorov-Sinai entropy: it is positive and finite for chaotic systems and stochastic processes with power-law power spectrum and it is infinite for "wild" stochastic processes like white noise. Once again, stabilization of K_2 for a low value of N_0 is a good symptom for the presence of a strange attractor.

Often times the use of correlation dimension leads to inconclusive discrimination between chaos and stochasticity. This happens because the values of ν_n may be quite sensitive to the number of points used to fit the power law. In order to circumvent these difficulties, other dimension algorithms have been introduced in the literature. The *false nearest neighbors* algorithm of Kennel et al. (1992) relies on the observation that on a true attractor, neighboring points should remain close dynamically. The idea is then to follow the evolution of the points in phase-space and calculate the number of those that appear to be close but which in reality are far in higher dimensions. The proper embedding dimension is then identified as the phase-space dimension for which the percentage of false neighbors remains close to zero.

Confirmation of chaotic behavior relies on the exponential divergence of orbits originating very close within the strange attractor. A positive largest Lyapunov exponent for the records confirms such behavior. This is computed by following an infinitesimal N_0 sphere of initial conditions, Wolf et al. (1985). As time passes, the sphere evolves into an ellipsoid and one may compute the growth of the largest principal axis $P_i(t)$ to arrive at the Lyapunov exponent λ_1:

$$\lambda_1 = \lim_{t \to \infty} \frac{1}{t} log_2 \left(\frac{P_i(t)}{P_i(0)} \right). \tag{24}$$

K_2 is a lower bound of the sum of all positive Lyapunov exponents.

3.2.2 A High Resolution Storm in Boston

Figures 15, 16 and 17 compare relevant statistics of the observed and predicted records from Boston. These results correspond to the ones given earlier in Table 2. As may be seen and as previously mentioned, the kind of fractal-multifractal representation found for the storm in Boston is comparable to the one already reported for the Iowa3 storm gathered in Iowa City, i.e. Figures 11 to 13.

Observe that despite the 1990 data points in Boston, the fractal-multifractal projection give reasonably close fittings of both the autocorrelation function and power spectrum of the actual data. Notice the similarity in the shapes of these functions, with the autocorrelation of the actual data being rougher than the one predicted by the fractal-multifractal approach; and with the power spectrum of the predicted records exhibiting a less stable power law behavior that the actual records.

In terms of the data histogram $(f(dy))$, even though the predicted and real shapes do not match perfectly, there is indeed a good visual agreement and good fit of the moments as previously reported in Table 2. Overall, the moments in both time and intensity axis are very well preserved as seen in Figure 17 for time moments of orders up to 15, and intensity moments of orders up to 10.

As seen with the mass exponents in Figure 17 and the multifractal spectra for the observed and predicted storms given at the right hand corner of Figures 15 and 16, good agreement between real and predicted is only found on a region of exponents q and only for the left hand portion of the multifractal spectrum. As real and predicted mass exponents deviate for large magnitudes of the exponent q, the multifractal spectra of both series differs in both tails of the multifractal spectrum, see the Legendre relationships, equations (12) and (13). It is clear that the right hand portion of the predicted multifractal spectrum is not preserving what is present in the data, even while changing the number of regression points nr. Overall, the entropy dimension, an stable qualifier of the spectrum, is well preserved by the fractal-multifractal measure. This is particularly true for regressions made with 4 and 7 resolutions.

A chaotic analysis for both of the Boston records is included in Figures 18 to 21. Figures 18 and 20 include the correlation dimension analysis and K_2 entropy calculations using a delay τ obtained from the first local minimum of the autocorrelation function of the real records (i.e. 23). These figures include the following information:

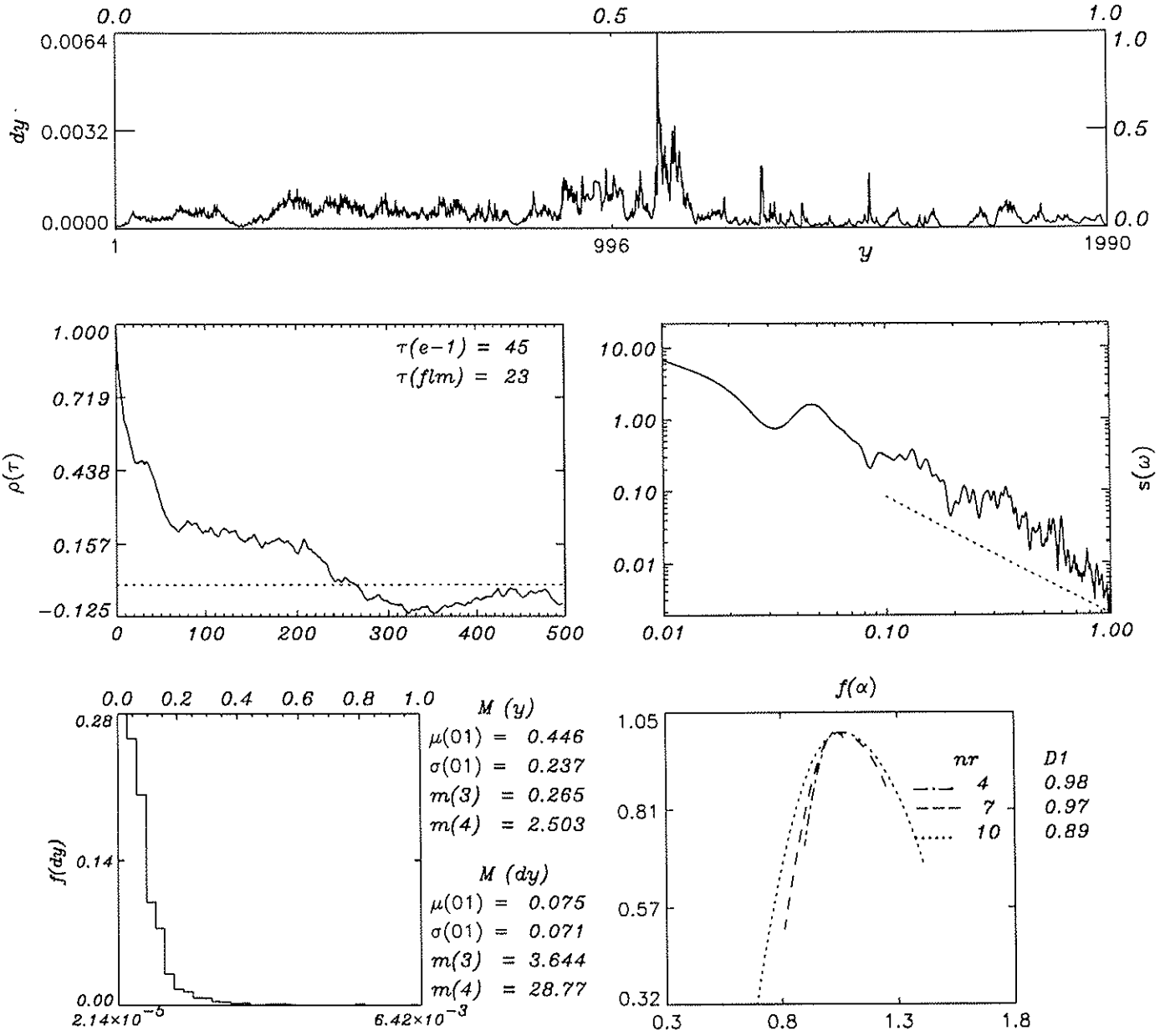

Figure 15: Statistics for observed storm in Boston: autocorrelation ($\rho(\tau)$), power spectrum ($S(\omega)$), data histogram ($f(dy)$), and multifractal spectrum ($f(\alpha)$).

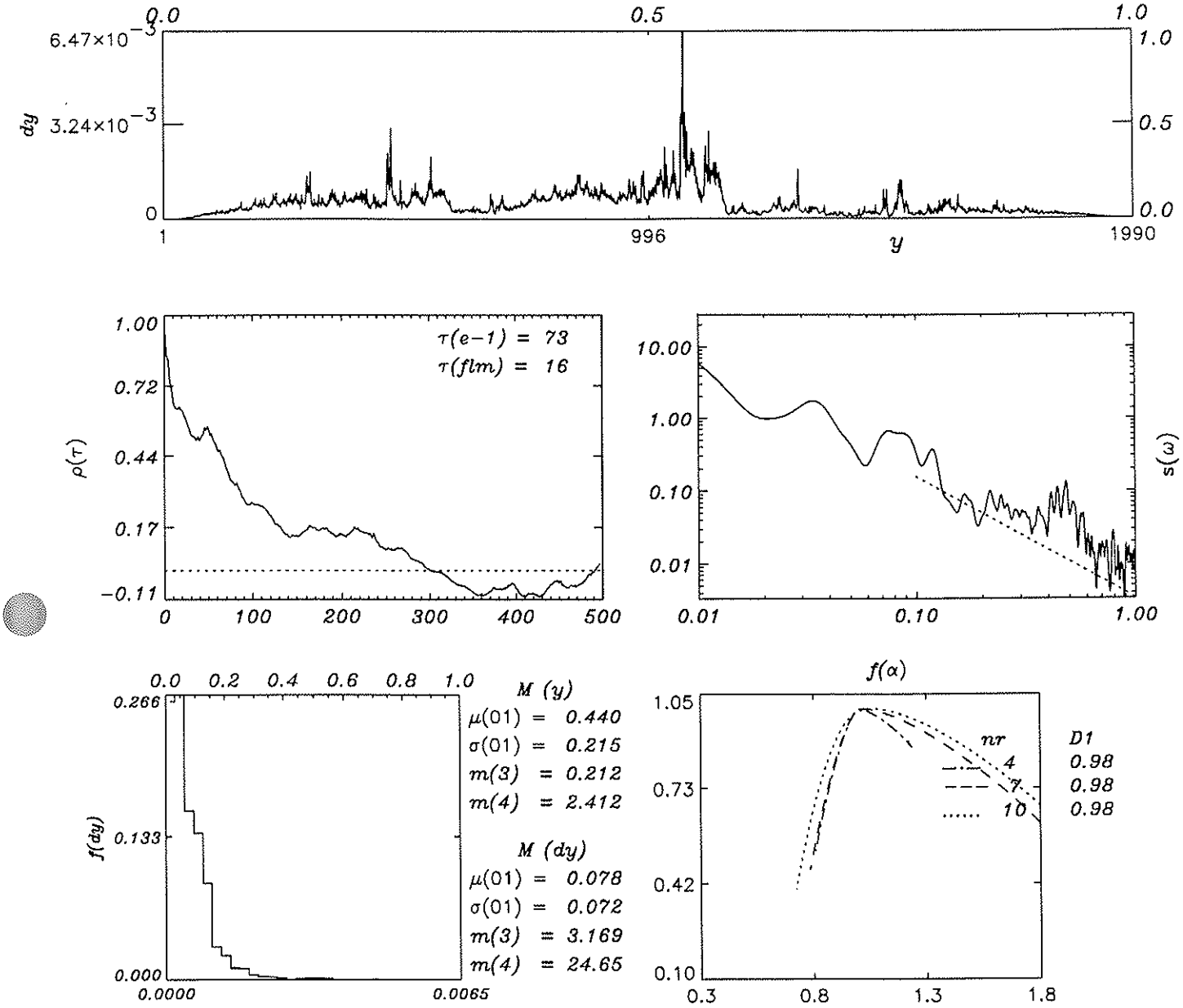

Figure 16: Statistics for predicted storm in Boston: autocorrelation ($\rho(\tau)$), power spectrum ($S(\omega)$), data histogram ($f(dy)$), and multifractal spectrum ($f(\alpha)$).

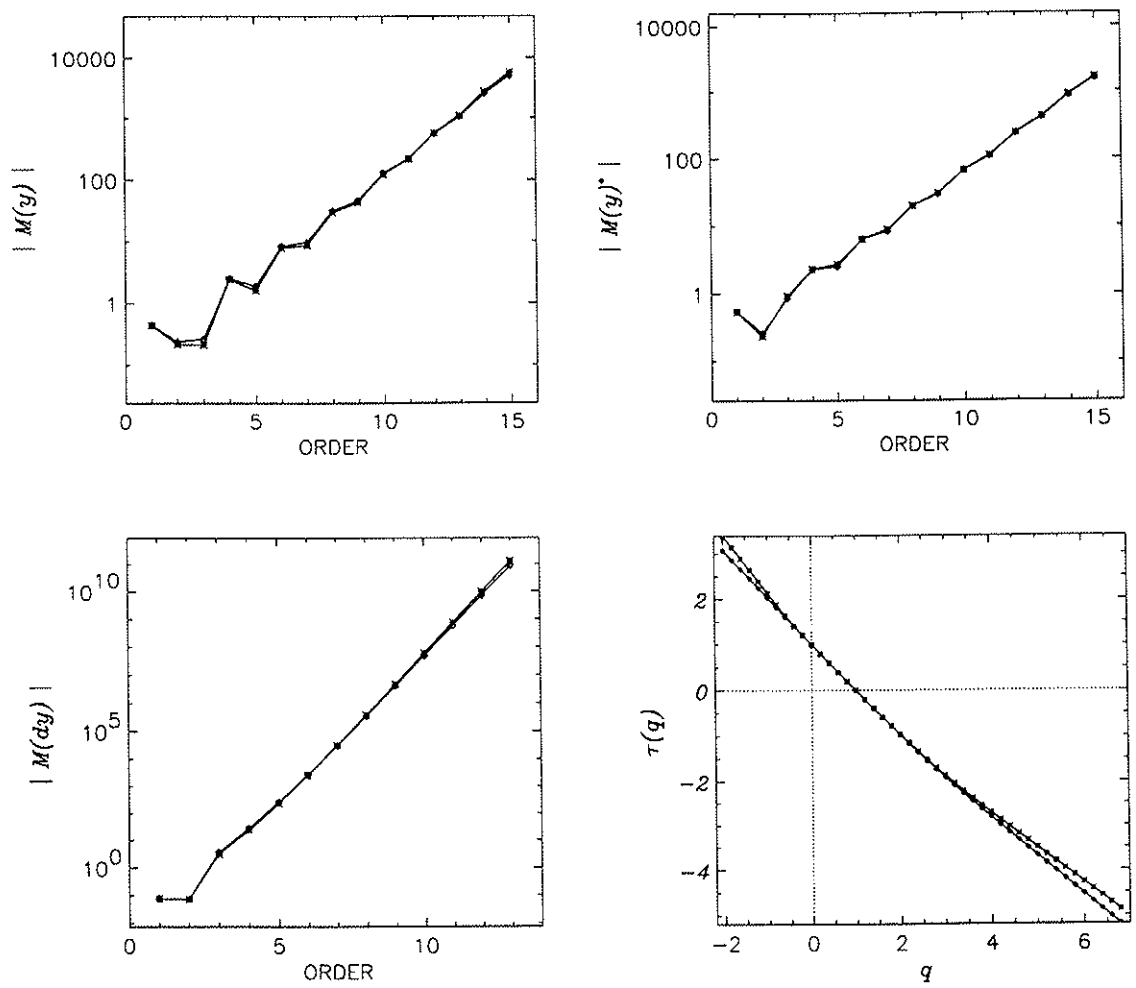

Figure 17: Moments for observed and predicted (*–*) storm in Boston: central moments in time ($M(y)$), modal moments in time ($M(y)^*$), central moments in intensity axis ($M(dy)$), and mass exponents ($\tau(q)$).

(a) the phase-space correlation functions $C_N(r)$,

(b) the local slope of $C_N(r)$ (computed via lag-one differences),

(c), (d), and (e) the correlation dimensions ν_N computed for five large, five intermediate, and five small values of the distance r, respectively. Such values are indicated on the upper correlation function curve (i.e. $N = 2$) and are found via a regression of three successive points ending with the symbol in question, e.g. the values reported for ν_n and symbol "+" are obtained employing $C_N(r)$ values for distances indicated by "$\triangle$", "$*$", and "+",

(f) the average $K_2(N)$ entropy found for the "stable" region in the correlation function slope and the band of plus and minus one standard deviation, and

(g) the average value of $1/K_2(N)$ and its corresponding band of one standard deviation.

As may be seen on part (a) of Figures 18 and 20, the computed correlation functions for both observed and predicted records are not perfect straight lines in log-log scale. This leads to stable and unstable local slopes as indicated in part (b) of these graphs. While the actual data leads to a slope valley between two mounds, the local slopes on the predicted records show only one mound and smooth behavior for larger distances. Notice from parts (c), (d) and (e) of Figure 18 that the real data exhibits stable correlation dimension estimates only in the intermediate zone, leading to a correlation dimension $D(2)$ of 3.68, see for example the graph with symbol "$\times$" in Figure 18(d). The predicted records, on the other hand, also lead to stable behavior and close correlation dimension of 3.44, see Figure 20(e) and symbol "$*$". These values are quite close to the 3.78 reported for this storm by Rodriguez-Iturbe et al. (1989).

The $K_2(N)$ entropy analysis yields inconclusive results for both the real and predicted storms. As may be seen in Figures 18 and 20(f), (g), K_2 remains positive for all embedding dimensions N, but no apparent stabilization of either $K_2(N)$ or its inverse is attained. The short length of the time series precludes a more complete analysis regarding this attribute. Notice however that the behavior of real and predicted entropies is quite similar.

Figures 19 and 21 verify the correlation dimension results by bounding the optimal embedding dimension using the method of false neighbors (Kennel et al., 1992). These figures also include the largest Lyapunov exponents under alternative conditions (Wolf et al., 1985).

Notice that the percentage of false neighbors behaves very similarly for both real and predicted records. As may be seen in Figures 19 and 21, for delays τ which range from 8 to 32, there is a marked decrease in false neighbors as the embedding dimension is increased from 2 to 4. At this stage, the percentage of false neighbors falls in all cases below 10%, and only a mild rise is observed after. These results clearly support the validity of the correlation dimension values given before.

The largest Lyapunov exponent (λ_1) for both real and predicted series are given in Figures 19 and 21 for an optimal embedding of $N_0 = 4$ and for a couple of plausible delays τ. The results for the real data are clear. A positive Lyapunov exponent is found for both delays considered. For the predicted records the Lyapunov exponents vary in character. For

the most of the time λ_1 gives positive values which signify chaotic behavior, but there are series durations for which negative values are found. Overall, the behavior of both real and predicted records is similar in relation to the largest Lyapunov exponent: notice that the scales on both cases is quite close and that indeed positive values are found, compare in particular the cases when $\tau = 16$.

In order to avoid issues related to the small length of the time series, the previous chaotic analysis was also carried with simulated records having 16,384 values. The study confirmed the chaotic nature of the fractal-multifractal projection which nicely approximates the Boston data at the lower resolution. Once again a dimension close to 3.7 was found and the percentage of false neighbors came below 10% for 4 embedding dimensions. This time a positive largest Lyapunov exponent was found, even for the duration of the series.

3.2.3 Fractal-Multifractal Data Sets

The previous section illustrated that it is possible to have a deterministic data set generated via the fractal-multifractal procedure, which in turn results to be low-dimensional and chaotic. This was a bit surprising because determinism in the generated measure do not have to translate necessarily into chaotic behavior, e.g. it could also lead to deterministic non-chaotic behavior. In this section it will be shown that low-dimensional chaotic behavior is not the only exotic response. Specifically, it will be demonstrated that fractal-multifractal parameter combinations exist, whose corresponding projections give "high-dimensional" and for all practical purposes "stochastic" behavior. This unexpected property is welcomed as it allows the fractal-multifractal procedure to have a wide range of *deterministic and stochastic* applications.

Figures 22 and 23 show the construction of two typical data sets which will be used to illustrate low and high-dimensional behavior. They are obtained as projections in y (dy) of simple wires in two dimensions which pass by three-point geometries (termed "b" and "a" and defined on the headings of Figures 22 and 23, respectively). The two scaling parameters are also reflected in the names of the data sets: -0.5 and 0.7 for the measure dyb-573, and 0.7 and 0.3 for dya736. As may be seen, the two measures come from parent binomial multifractal measures which have as intermittency parameters 0.3 and 0.6, respectively. These parameters are encrypted in the last numbers on the names of the two measures.

As may be observed on Figures 22 and 23, the measure dya736 comes from a wire which requires less ink than the one needed to generate dyb-573. In fact, using equation (3), it may be shown that the former wire has fractal dimension one, while the latter has a fractal dimension of about 1.26. As a consequence, the wire "xya73" filters the intermittencies of the parent binomial multifractal less than the wire "xyb-57". This leads, as clearly seen on Figures 22 and 23, to a measure dya736 which inherits more of the features of its parent binomial multifractal than dyb-573. Of course, this is simply summarized by noticing that dya736 has a "wilder" appearance than dyb-573.

Figures 24 and 25 confirm the different nature of the data sets. The two series (having both 16,384 points) reveal basic differences in all their statistical and multifractal attributes. The autocorrelation functions differ in their shape and basic scale, with the wilder dya736 having a much smaller correlation length than dyb-573. This is clearly seen in terms of

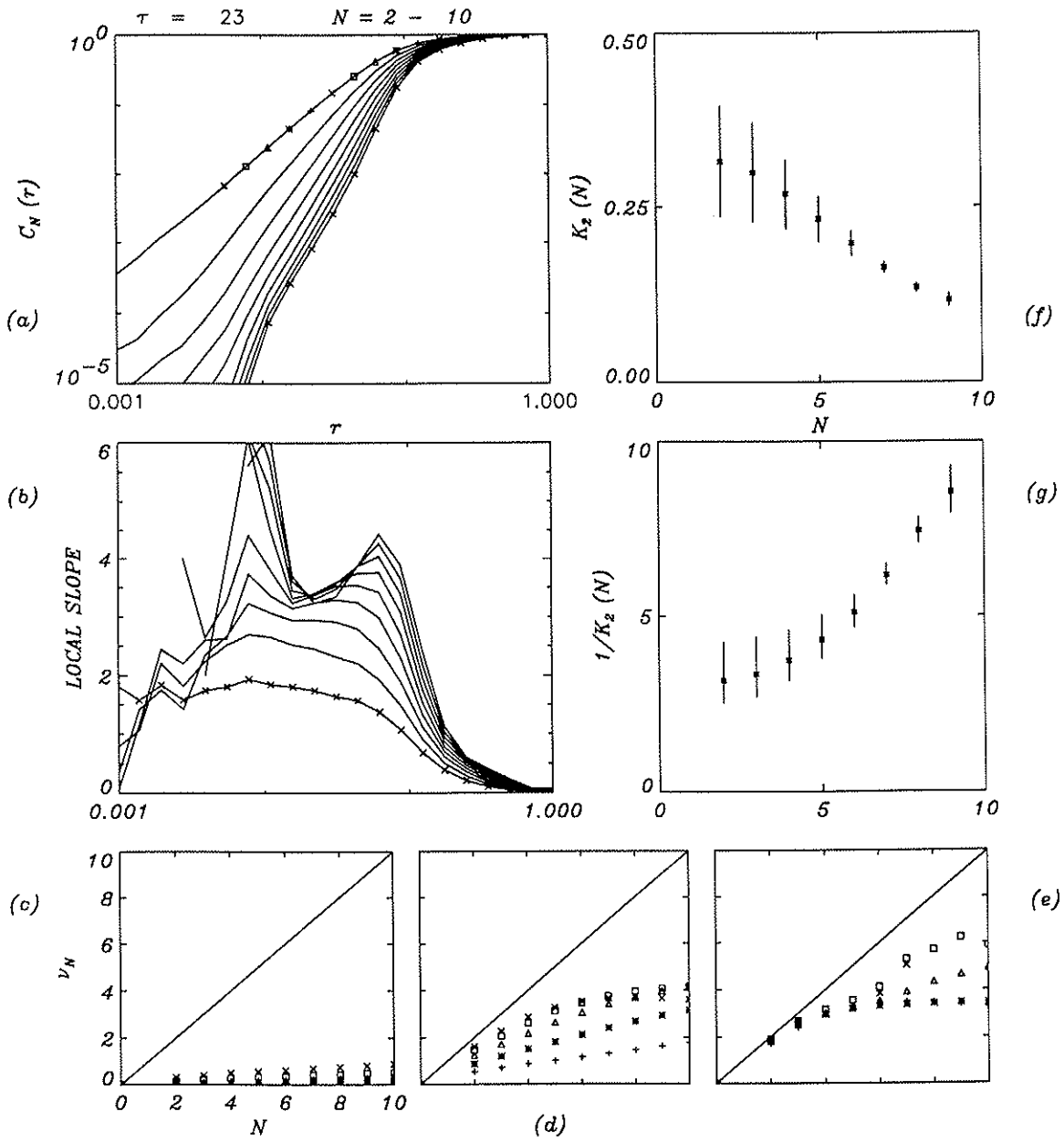

Figure 18: Observed storm in Boston correlation dimension and K_2 entropy. (a) phase-space correlation functions, (b) local slopes of correlation functions, (c), (d), and (e) correlation dimensions for five large, five intermediate and five small distances r as indicated from right to left on the uppermost correlation function in (a) by the symbols $+$, $*$, $\triangle$, $\square$ and $\times$, (f) K_2 mean entropy and one standard deviation band, and (g) $1/K_2$ and one standard deviation band.

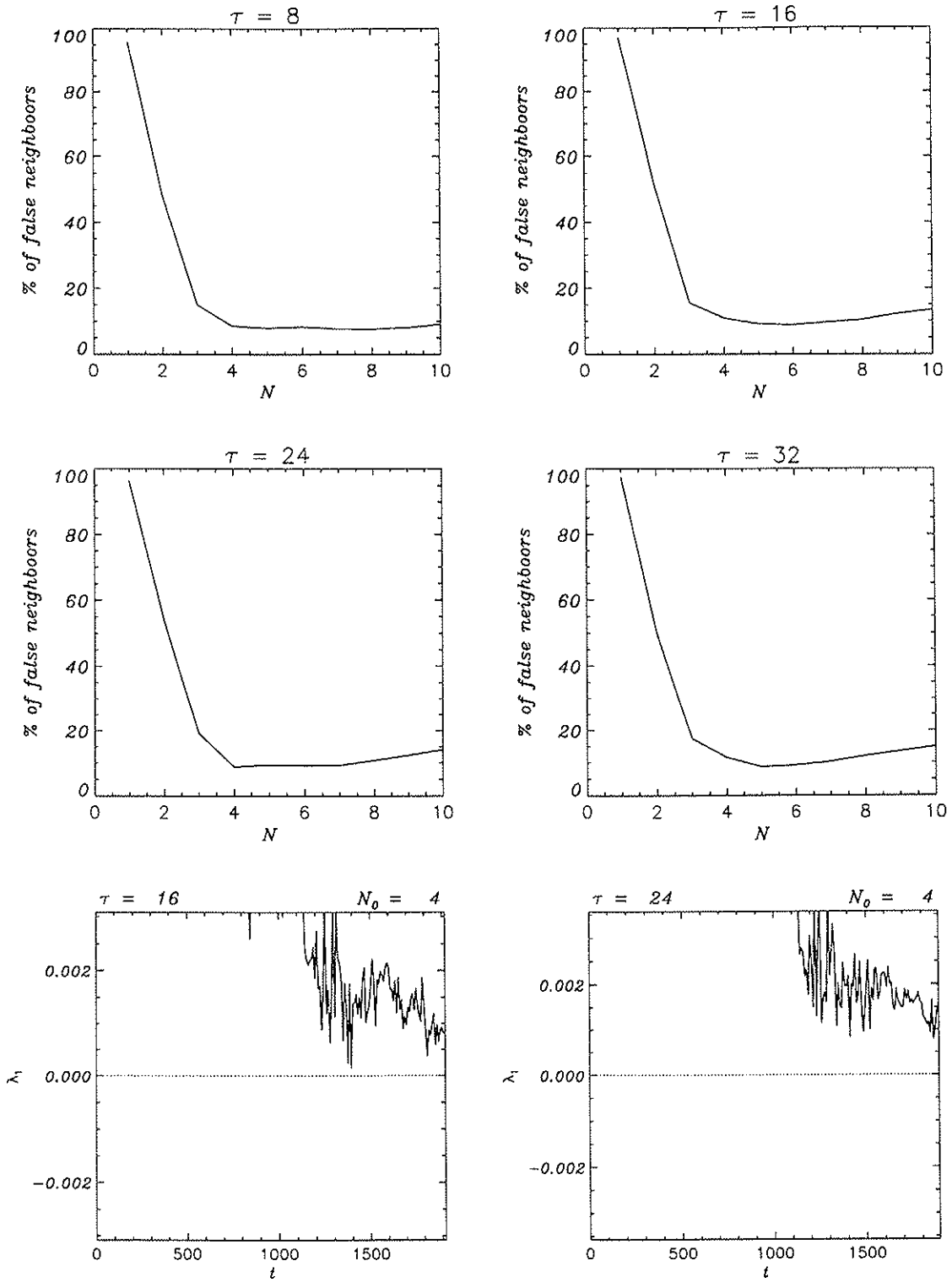

Figure 19: Observed storm in Boston: false neighbors for alternative delays (τ) and largest Lyapunov exponent for alternative dimensions (N_0).

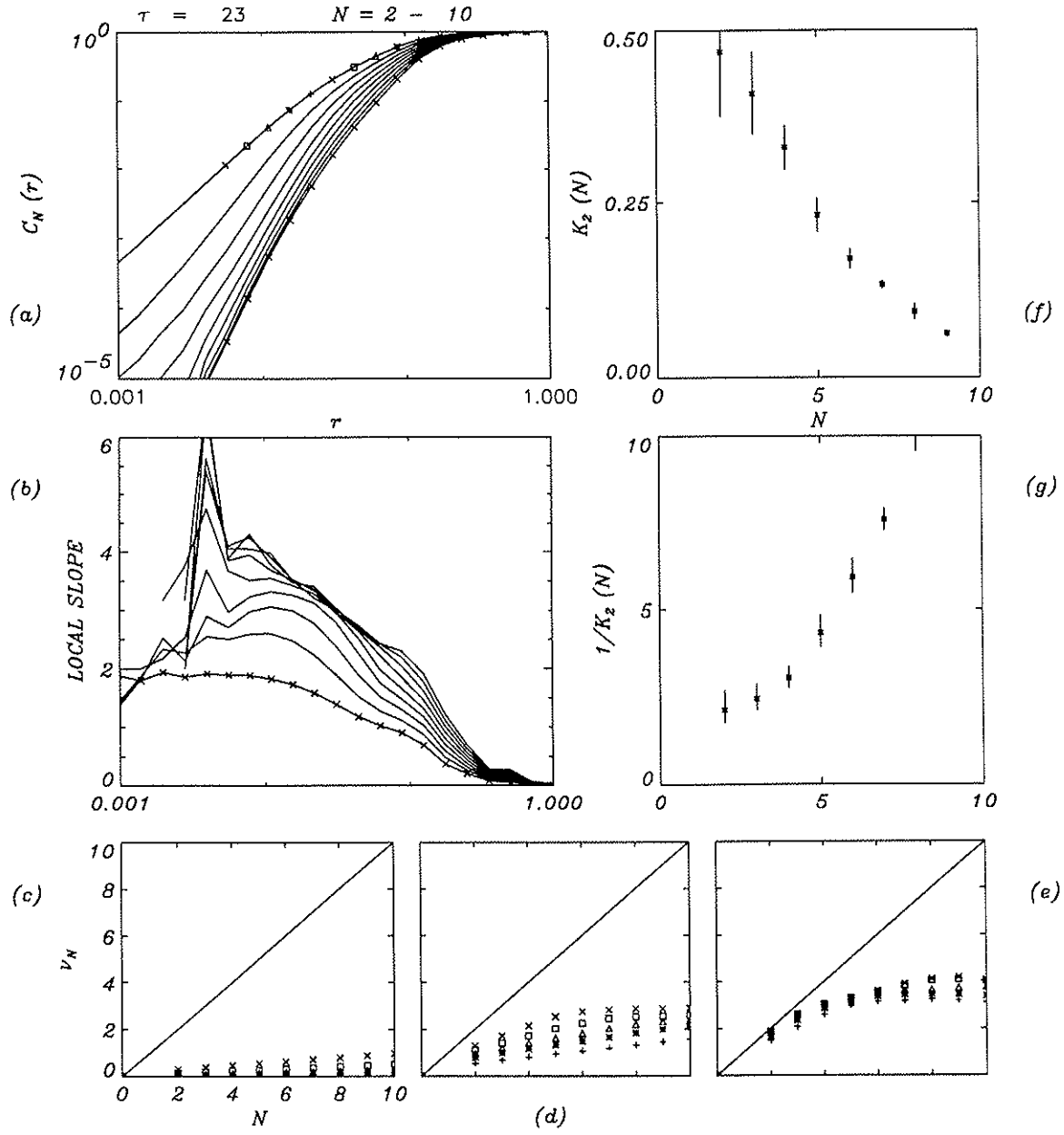

Figure 20: Predicted storm in Boston correlation dimension and K_2 entropy. (a) phase-space correlation functions, (b) local slopes of correlation functions, (c), (d), and (e) correlation dimensions for five large, five intermediate and five small distances r as indicated from right to left on the uppermost correlation function in (a) by the symbols $+$, $*$, $\triangle$, $\square$ and $\times$, (f) K_2 mean entropy and one standard deviation band, and (g) $1/K_2$ and one standard deviation band.

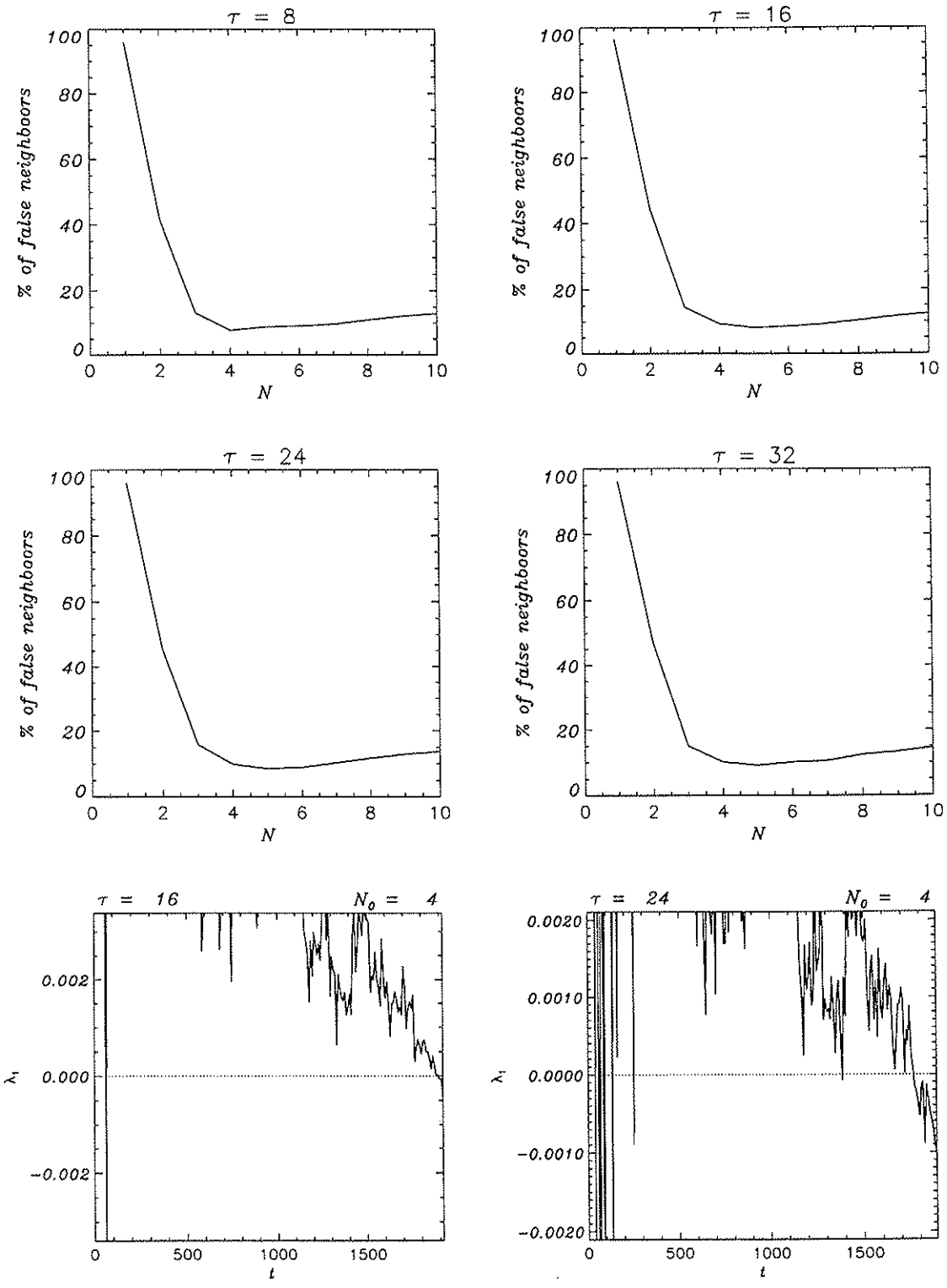

Figure 21: Predicted storm in Boston: false neighbors for alternative delays (τ) and largest Lyapunov exponent for alternative dimensions (N_0).

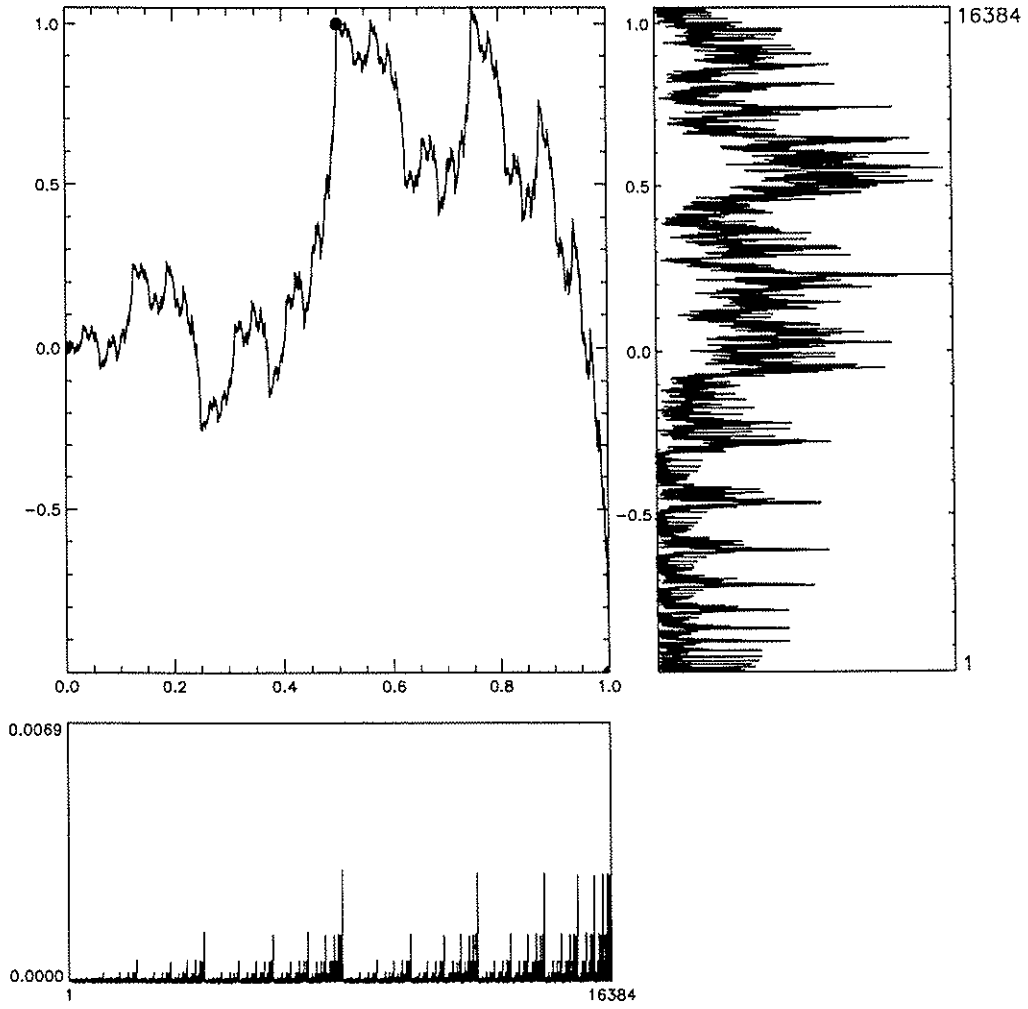

Figure 22: Measure dyb-573. Fractal-multifractal parameters: (a) localization, {(0, 0), (0.5, 1), (1, -1)}, (b) regularity, -0.5, 0.7, (c) intermittency: 0.3, 0.7.

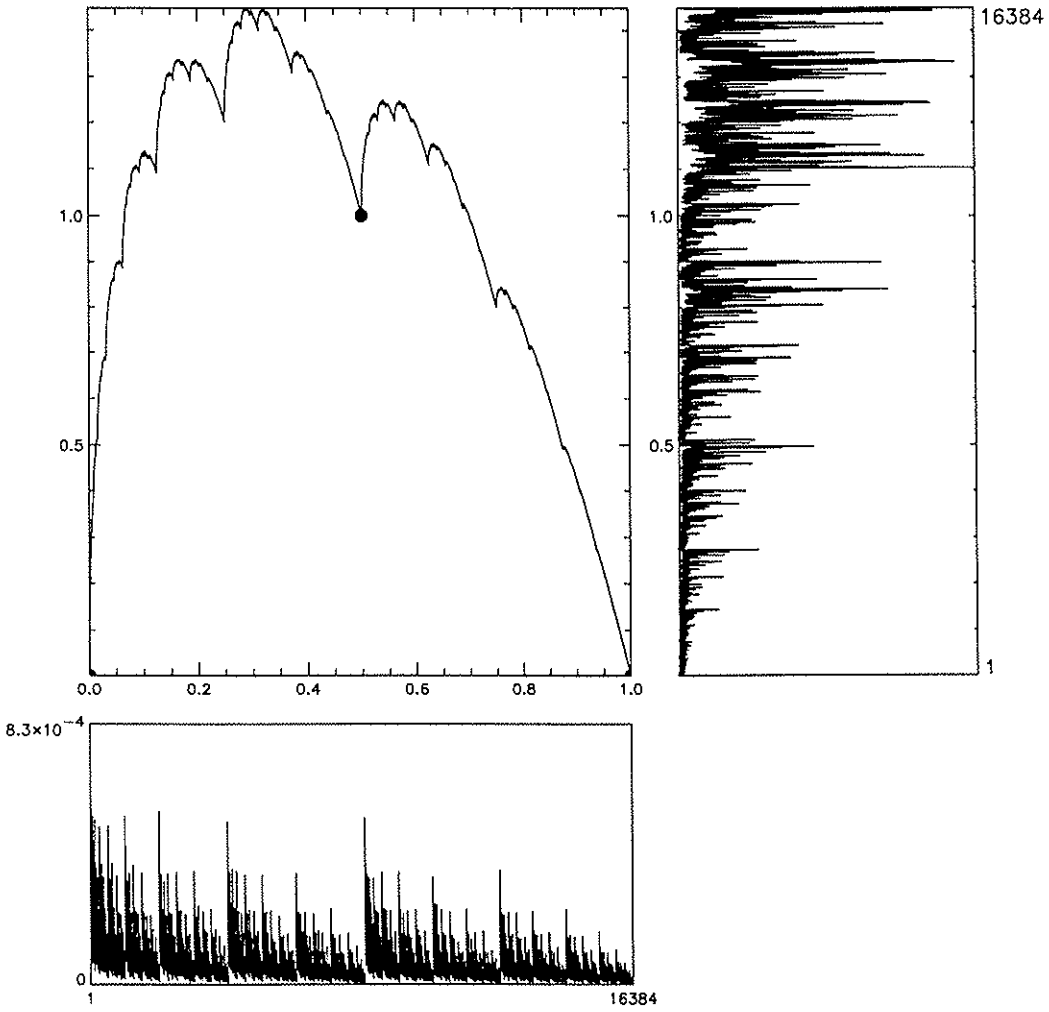

Figure 23: Measure dya736. Fractal-multifractal parameters: (a) localization, {(0, 0), (0.5, 1), (1, 0)}, (b) regularity, 0.7, 0.3, (c) intermittency: 0.6, 0.4.

the time delays corresponding to the correlation e^{-1} and the autocorrelation's first local minimum. The difference in shape between the two data sets is reflected by the shapes of the corresponding histograms. While dya736 has ordinates which remain close to the origin, dyb-573 gives a broader set of values which result in a less positively skewed histogram. Although the spectral density function exhibits power law behavior in both cases, the wilder set dya736 has an exponent of 1.19 which is less than the 1.28 found for dyb-573. This is also consistent with the degree of irregularity of the two series. Finally, the difference in intermittency is also captured by looking at the multifractal spectrum of both data sets. In particular, the information dimensions $D1$ (for alternative resolutions used on the calculation of mass exponents nr) for dya736 all equal to 0.95, confirm that such a measure has an emptier domain than dyb-573, which has a value closer (0.98) to the fractal dimension of its domain, i.e. 1. In summary, the results on Figures 24 and 25 corroborate what is seen visually: although both series are deterministically generated, dya736 may be termed more erratic and less predictable than dyb-573.

A complete chaotic analysis was carried out on these and other simulated series. Figures 26 and 27 show the correlation dimension, K_2 entropy, false neighbors and largest Lyapunov exponent analysis for dyb-573, while Figures 28 and 29 give the same information for the measure dya736.

As may be seen on part (a) of Figure 26, the computed correlation functions for dyb-573 using 128 as delay for phase-space reconstruction were not perfectly straight lines in log-log scale. However, part (b) on the same figure shows a clear plateau in which the correlation function slope stabilizes. As may be seen on part (b) and corroborated in intermediate zone (d) using as key symbol "+", there is stable correlation dimension of about 5.2. Although the corresponding $K_2(N)$ entropy yields positive values for up to 20 embedding dimensions, no stable asymptotic K_2 entropy could be inferred for the set, see Figure 26(f), (g). As found earlier with the data sets dealing with the Boston storm, the finite length of the series may be the reason. In any event, the obtained positive results for $K_2(N)$ do not disprove the possible chaotic behavior for dyb-573 as suggested by the correlation dimension analysis. It should also be remembered that convergence to K_2 has been found to be slow in practice, Provenzale and Osborne (1991).

Figure 27 verifies the correlation dimension results by computing an upper bound to the optimal embedding dimension using the method of false neighbors, and includes information on the largest Lyapunov exponent for the reconstructed flow. Notice that the percentage of false neighbors analysis for dyb-573 suggests indeed an embedding dimension on the vicinity of 5 or 6. This is true for a variety of delays, and in particular for $\tau = 128$ as used on the correlation dimension analysis. As seen in relation to the largest Lyapunov exponents, a clearly positive value is found when the embeddings are made made of 5 and even 4 coordinates. These results do confirm the inferred chaotic nature of the deterministic measure dyb-573.

Figure 28 contains the correlation dimension and K_2 entropy analysis for the "wild" measure dya736. As found with dyb-573, the computed correlation functions for dya736 (using now a phase-space reconstruction delay of 16) were hardly straight lines in log-log scale. This lead to two zones in relation to their local slopes: one apparently stable for large

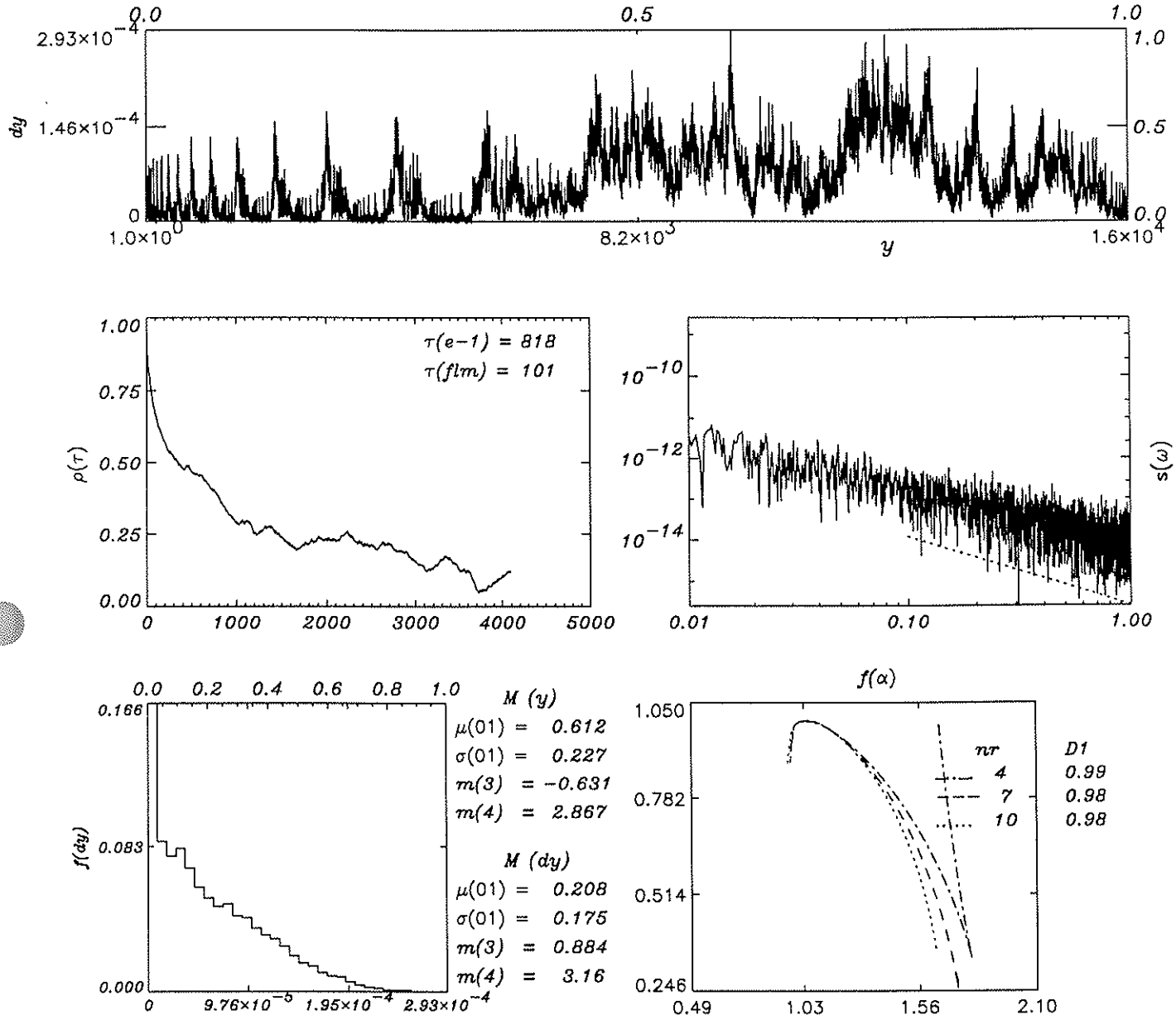

Figure 24: Statistics for measure dyb-573: autocorrelation ($\rho(\tau)$), power spectrum ($S(\omega)$), data histogram ($f(dy)$), and multifractal spectrum ($f(\alpha)$).

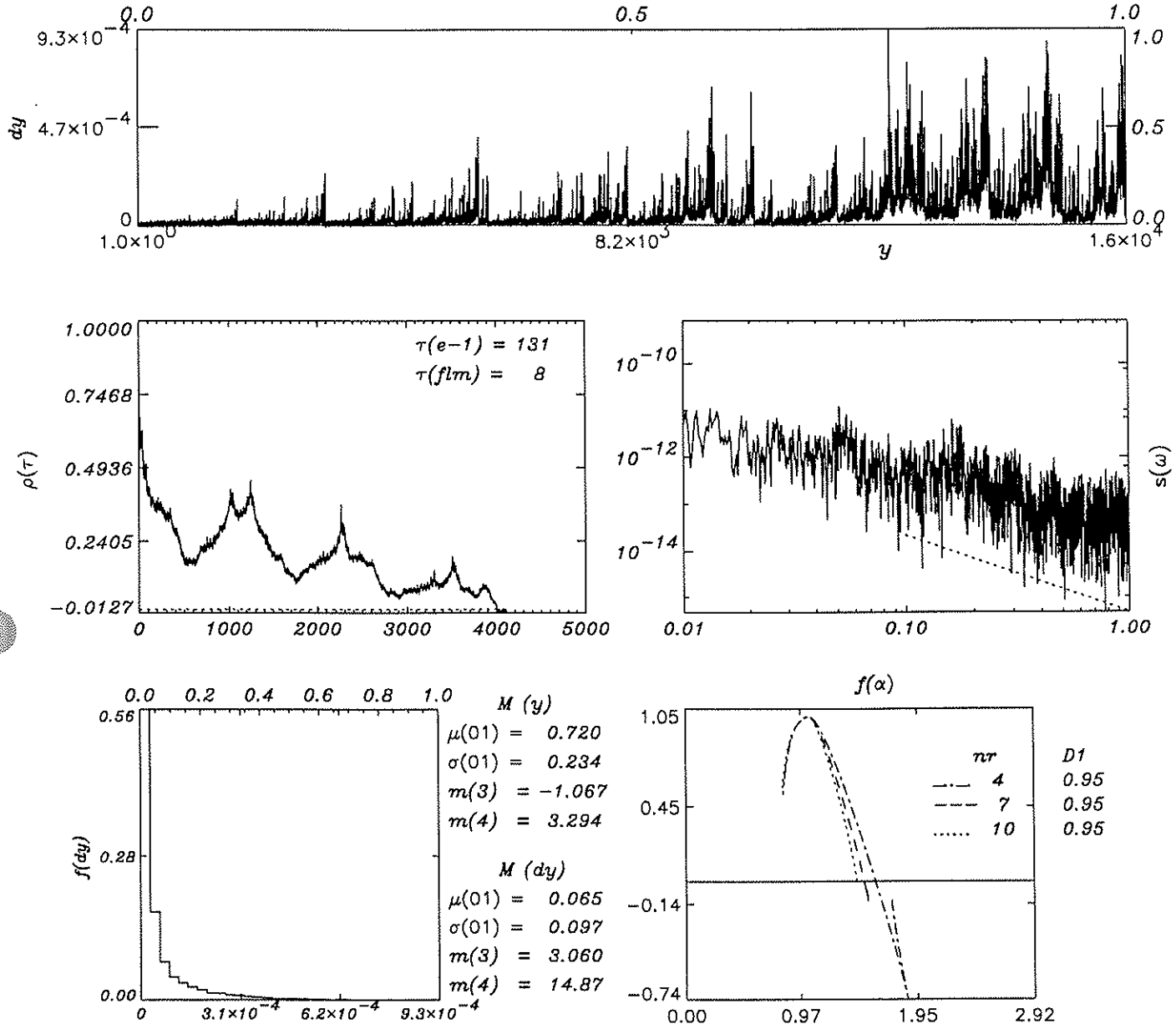

Figure 25: Statistics for measure dya736: autocorrelation ($\rho(\tau)$), power spectrum ($S(\omega)$), data histogram ($f(dy)$), and multifractal spectrum ($f(\alpha)$).

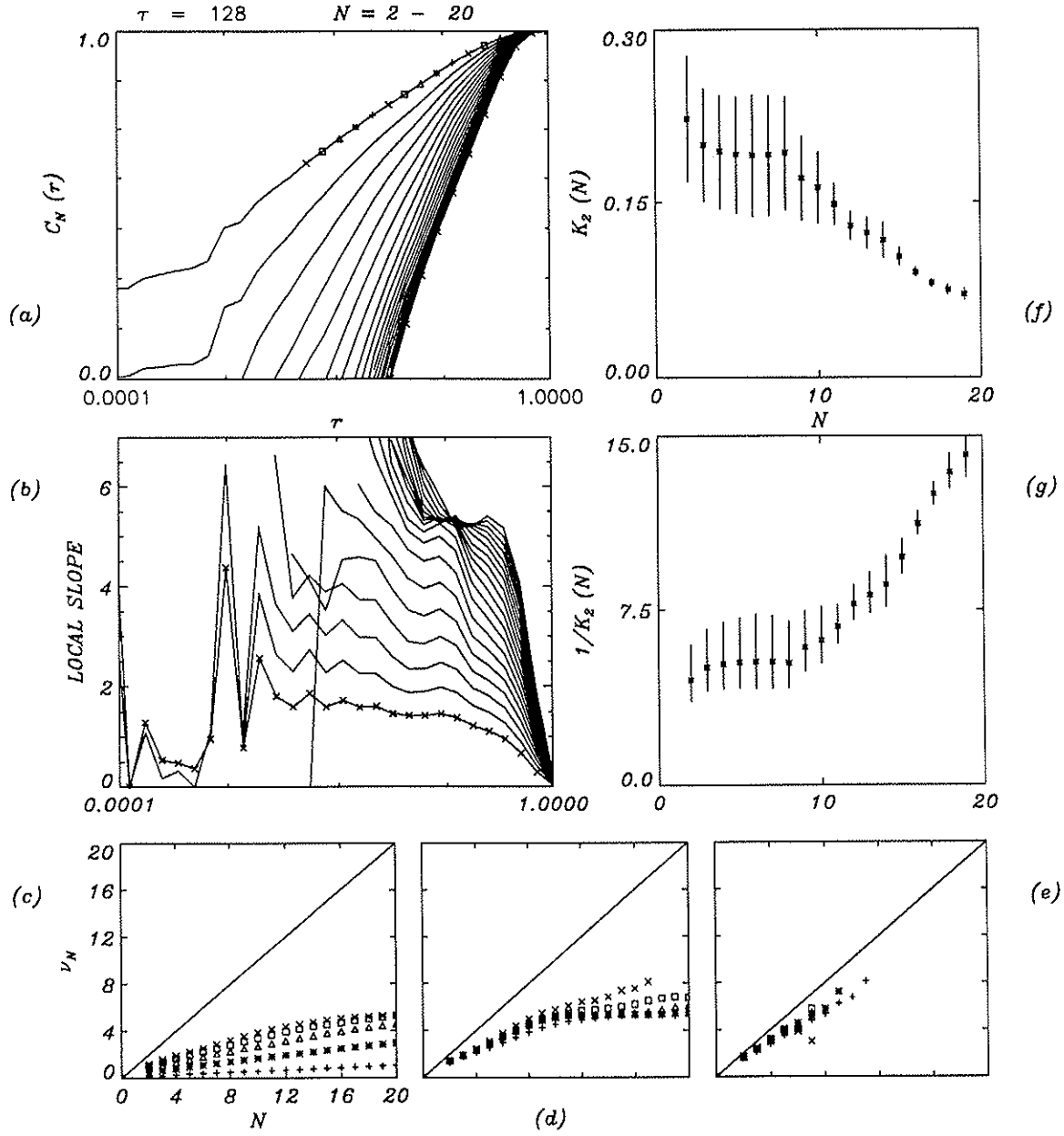

Figure 26: Measure dyb-573 correlation dimension and K_2 entropy. (a) phase-space correlation functions, (b) local slopes of correlation functions, (c), (d), and (e) correlation dimensions for five large, five intermediate and five small distances r as indicated from right to left on the uppermost correlation function in (a) by the symbols $+$, $*$, $\triangle$, $\square$ and $\times$, (f) K_2 mean entropy and one standard deviation band, and (g) $1/K_2$ and one standard deviation band.

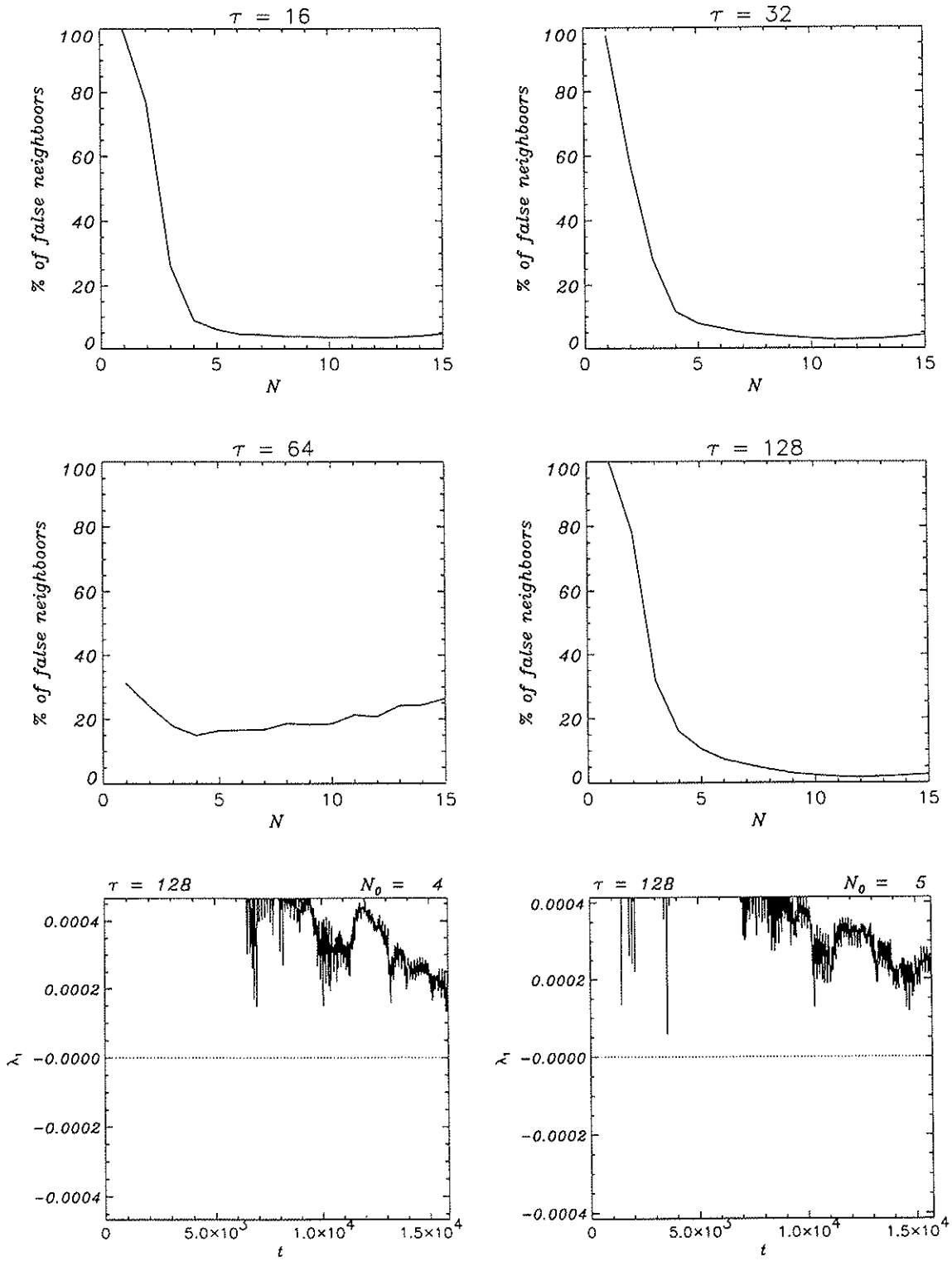

Figure 27: Measure dyb-573 false neighbors for alternative delays (τ) and largest Lyapunov exponent for alternative dimensions (N_0).

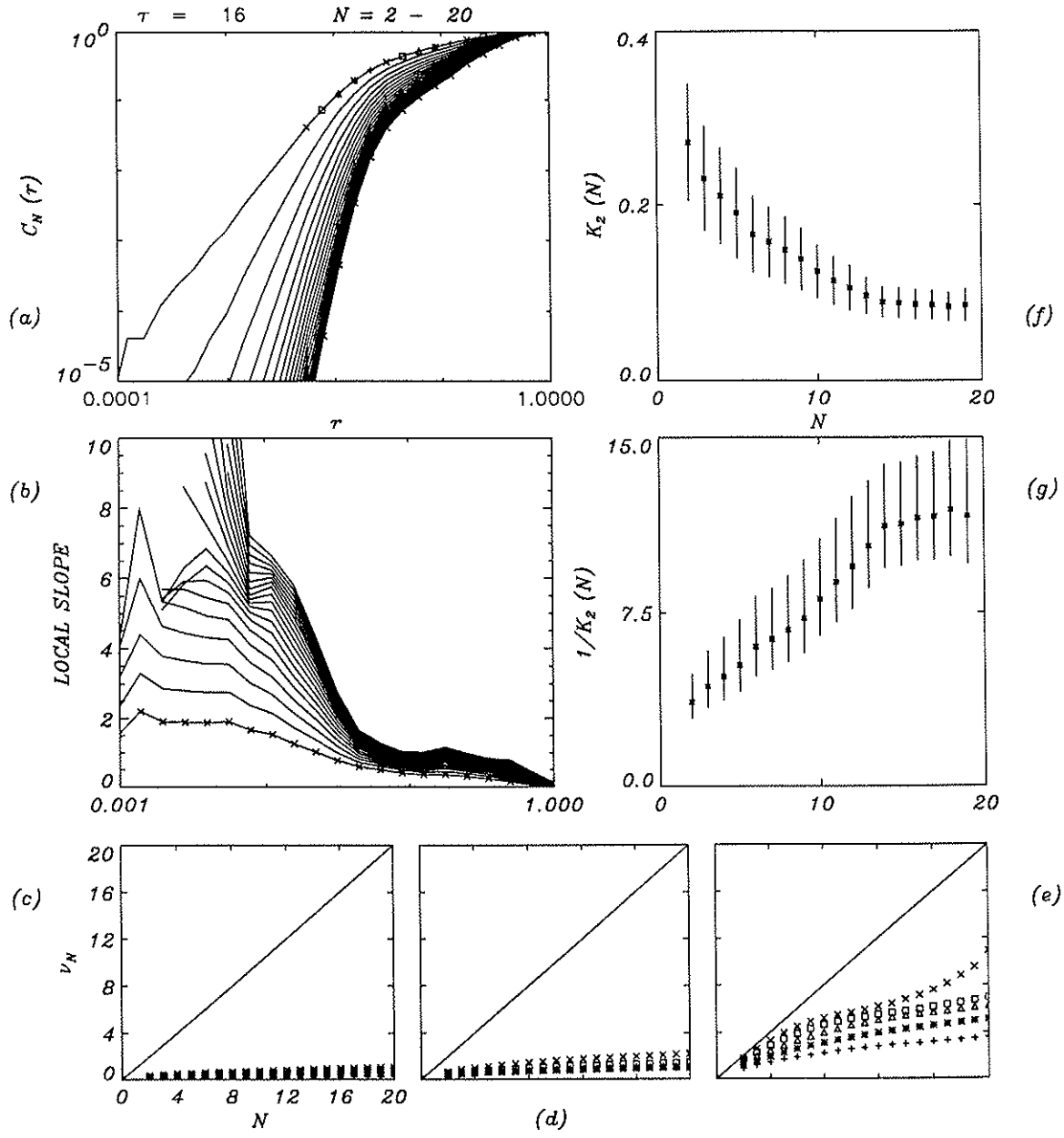

Figure 28: Measure dya736 correlation dimension and K_2 entropy. (a) phase-space correlation functions, (b) local slopes of correlation functions, (c), (d), and (e) correlation dimensions for five large, five intermediate and five small distances r as indicated from right to left on the uppermost correlation function in (a) by the symbols $+$, $*$, $\triangle$, $\square$ and $\times$, (f) K_2 mean entropy and one standard deviation band, and (g) $1/K_2$ and one standard deviation band.

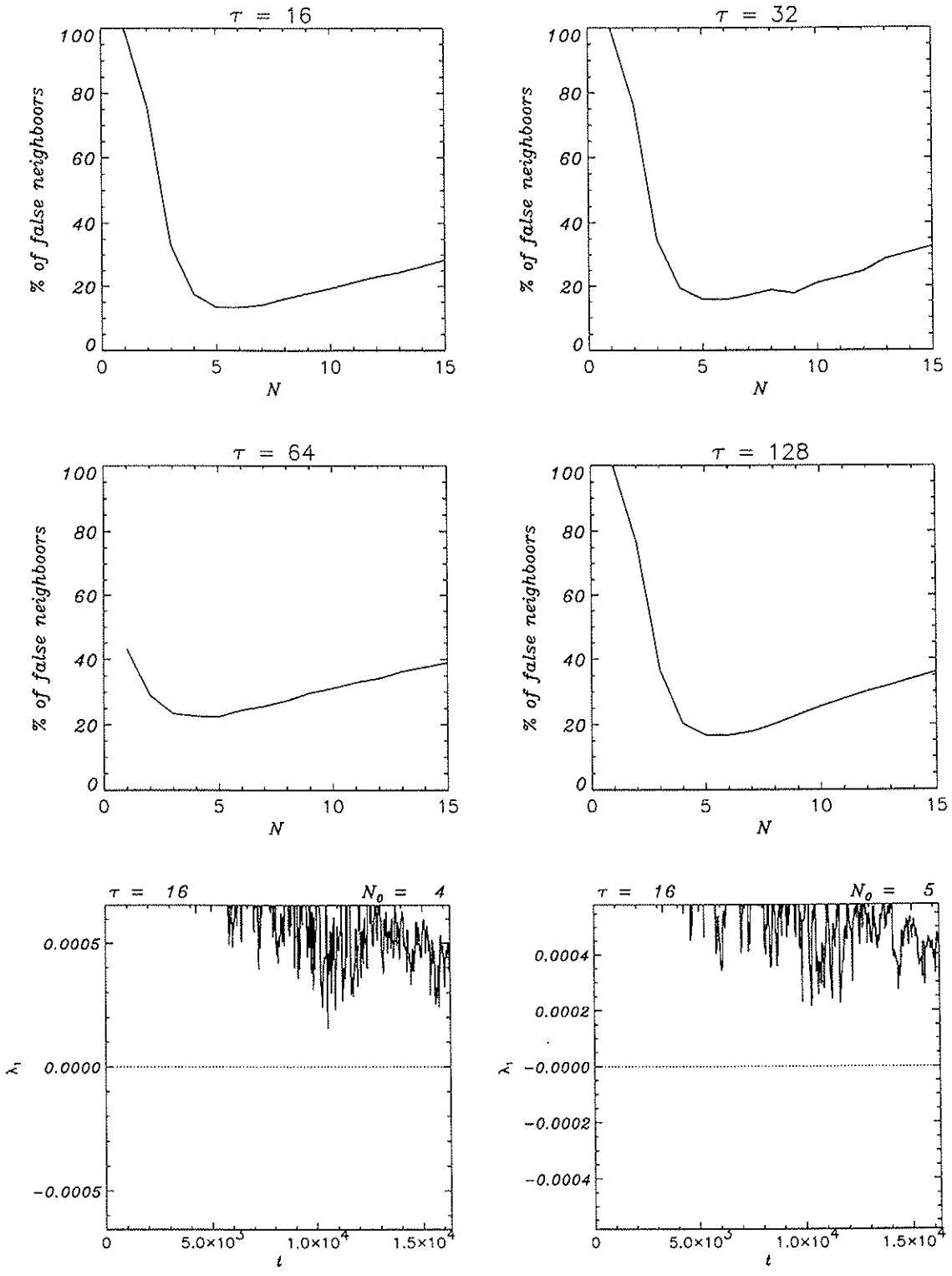

Figure 29: Measure dya736 false neighbors for alternative delays (τ) and largest Lyapunov exponent for alternative dimensions (N_0).

and some intermediate distances, and one clearly unstable as revealed by the increasing slopes for (some) intermediate and small distances r. However, part (b) on the same figure shows a clear plateau in which the correlation function slope stabilizes. While the stable zone would imply a stable correlation dimension of about 2, see Figure 28(c), (d); the unstable one gives asymptotes which range from 4 to 12, see Figure 28(e). Close scrutiny of all the correlation dimension curves (ν_N vs. N) reveal that none of the graphs do attain a clear asymptote. In fact, it is not hard to see that those graphs exhibit a monotonically increasing trend which prevents a proper definition of the correlation dimension $D(2)$. These results, and in particular the behavior seen at small distances r on Figure 28(e), suggest that dya736 may not qualify as low-dimensional and chaotic.

An interesting stabilization was found in relation to dya736 in regards to the $K_2(N)$ entropy, see Figure 28(f), (g). This attribute, which was calculated based on distances that correspond to the results of Figure 28(e), i.e. for small distances r, appears to reach an asymptote at about $N = 14$ for K_2 of about 0.09. This fact confirms the complexity of the measure dya736. It also suggests that the deterministically generated measure dya736 may indeed be chaotic but having a high number (14) of degrees of freedom.

False neighbor and largest Lyapunov exponents analysis for dya736 is found in Figures 29. As may be seen, the percentage of false neighbors does not become lower that 15% for a variety of time delays τ. This is clearly the case for values of the embedding dimension that are very low, i.e. 2, 3 (as may have been falsely suggested by Figure 28(c), (d)) and for large values of 14, or 15 (as may be suggested by the stable K_2 entropy in Figure 28(e)). Although there is a plateau in the percentage of false neighbors for dya736, the "low" values are not maintained when additional phase-space coordinates are added. The same kind of results were obtained when the reconstruction delay was reduced to 8. The fact that the percentage of low neighbors is never close to zero, and the observed growth in the percentage of false neighbors, indicate that dya736 can not be classified as a low-dimensional system.

The positive largest Lyapunov exponents for dya736 confirm that such time series is complex, see Figure 29. This results suggest that dya736 can be termed high-dimensional and "stochastic".

3.3 Rainfall in Space

To illustrate the potential of the fractal-multifractal representation to describe spatial rainfall data, Figure 30 shows several contour plots of joint derived measures that were obtained transforming binomial multifractal measures via a three-dimensional fractal interpolating function. The parameters (Θ) that were used and the corresponding binomial multifractal parameters p_n are shown in Table 6. All graphs, which are not meant to represent rainfall per se, share the first and last interpolating data points which are (0,0,0) and (1,0,0). Notice the wide variety of geometries that could be captured by means of the three-dimensional fractal-multifractal approach. Observe that depending on the parameter choice, these figures reflect situations that have both highly "intermittent" (multifractal) and anisotropic behavior, or "smooth" and seemingly isotropic behavior. Notice also that some of these graphs reflect data sets that are recognizable as appearing in hydrologic (rainfall) or geophysical applications. Observe that even though some of these figures may be considered "fractal", they do not

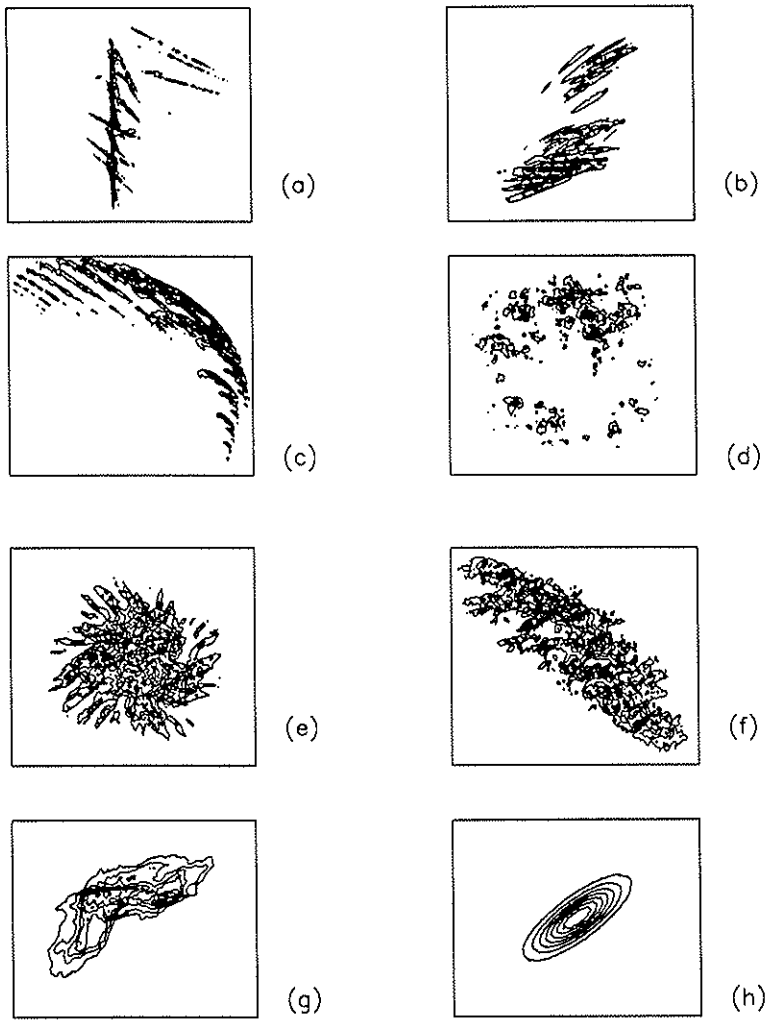

Figure 30: Examples of bivariate derived measures for parameters in Table 6.

exhibit mathematical self-similarity (self-affinity).

In the spirit of the paradigms mentioned in the introduction, it is plausible that a simple geometric-based dynamic description of hydrologic (geophysical) phenomena may be developed based upon the fractal-multifractal method. A new approach to dynamics may be drawn as follows. Instead of concentrating on (stochastic) partial differential equations which describe dynamics, one may study the evolution of geometric "*surrogate*" (fractal-multifractal) parameters which allow the encoding of successive snap-shots of hydrologic patterns. If in practice one finds a set of surrogate parameters which is small in size, one may literally *see* how patterns evolve without the need of partial differential equations.

That the proposed approach may work to describe the dynamics of rainfall patterns in space is illustrated in Figure 31. These simulations were obtained via the fractal-multifractal approach and the changes seen (clockwise) from frame to frame are due only to the variation

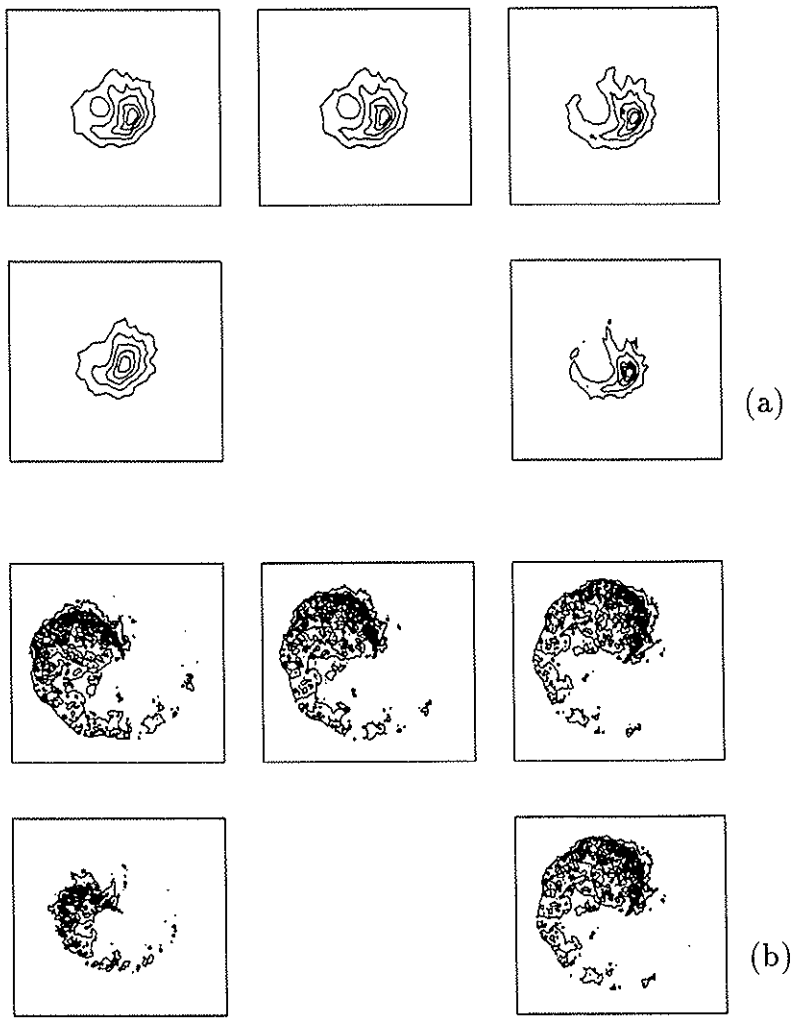

Figure 31: Plausible storm evolutions (clockwise).

Table 6: Set of data and parameters for Figure 30. (angles in degrees).

	Middle Point	First transformation				Second transformation				Weights	
	Coordinates	$r_1^{(1)}$	$\theta_1^{(1)}$	$r_1^{(2)}$	$\theta_1^{(2)}$	$r_2^{(1)}$	$\theta_2^{(1)}$	$r_2^{(2)}$	$\theta_2^{(2)}$	p_1	p_2
(a)	(0.5,0.2,1)	0.5	30	0.5	30	0.5	180	0.995	180	0.3	0.7
(b)	(0.5,0.3,1)	0.995	30	0.5	30	0.995	180	0.7	180	0.3	0.7
(c)	(0.4,0.4,1.2)	0.5	0	0.5	0	0.7	0	0.995	15	0.3	0.7
(d)	(0.5,0.2,1)	0.5	0	0.5	0	0.9	90	0.995	90	0.35	0.65
(e)	(0.5,-0.7,1)	0.995	30	0.5	30	0.995	270	0.7	270	0.4	0.7
(f)	(0.5,-0.7,1)	0.5	30	0.5	30	0.9	180	0.995	180	0.3	0.7
(g)	(0.5,0.3,1)	0.5	90	-0.995	90	-0.995	90	0.995	90	0.3	0.7
(h)	(0.6,0.2,1)	0.995	90	0.995	270	0.995	270	0.995	90	0.4	0.6

of 8 surrogate parameters. The continuity of the fractal-multifractal representation is key in this regard as nature exhibits precisely the same property. This implies that one should be able to encode nearby patterns (in time) via fractal-multifractal combinations which have nearby parameters. Moreover, it seems that one could use the same fractal-multifractal parameterization (e.g. with the same number of interpolating points and structure) for subsequent patterns.

It must be remembered that the multifractal measures used to drive the method are of importance in the field of turbulence. This implies that the observed patterns may be interpreted as *reflections* of turbulence. Clearly, this fact provides a reasonable physical statement: turbulence is ever present in hydrology (geophysics) and what we see is indeed related to it. The fractal-multifractal procedure ought to be thought on such light: what we see are reflections (transformations) of physico-chemical-biological (turbulent) mechanisms which take place within the appropriate medium (the atmosphere for rainfall).

Although it may be argued that geometry is not enough to characterize the rainfall process, it must be emphasized that natural complex geometries (as opposed to Euclidean ones) hardly repeat. There are no two clouds that are the same, but there are indeed several (spherical) soap bubbles that look the same. There are no two clouds that are just the same. They all have the property of being "clouds", but their *infiniteness* and *uniqueness* are ever present. This quality of natural patterns is preserved by the geometric representation. By varying its parameters, the fractal-multifractal procedure leads to an infinite number of distinct (but similarly looking) outcomes.

As previously pointed out, the measures given by the fractal-multifractal approach are easily found and are neither self-similar nor self-affine. That one can find patterns that look reasonable employing few surrogate parameters has been extensively illustrated in this report. All these complexity is accomplished without using differential equations or stochastic methods. As pointed out in the introduction, there is room for improvement when dealing with the dynamics of hydrologic (geophysical) systems. Even though the approach via

partial differential equations is physically correct, it is not uncommon to have situations in which the overall structure of the available records are not preserved. Of course this does not mean that the physical principles used are wrong, but rather that there are problems with: (a) the specification of boundary conditions and parameters, (b) the proper selection of a representative elementary volume, and (c) the"closure" problem in turbulence (Lesieur, 1990).

As with the physics of convection (Libchaber, 1982), which of course is described by partial differential equations, it is in the realm of the "New Physics" (Davies, 1989) that hydrologic phenomena may be understood by means of alternative approaches. If the fractal-multifractal procedure or a similar approach proves successful, simple expressions among the surrogate parameters may be discerned just by plotting them as a function of time. It is indeed conceivable that the "geometric effects" may be "filtered-out" when seen at the surrogate (geometric) level, and that simple expressions for the evolution of patterns may be obtained in terms of surrogate parameters of subsequent patterns. These expressions may provide (perhaps universal) laws which become explicit at the surrogate level. This would lead to a new approach to hydrologic (geophysical) dynamics. Given that diffusion, dispersion and advection are among the most important physical mechanisms taking place in nature, it is expected that such processes may be translated in terms of the surrogate parameters, which then will have an acceptable "physical" interpretation. It may be, however, that the important parameters are variables that are not to be measured in the field, but rather surrogates of measurable quantities.

Whether or not a procedure like the one proposed here is a *dual* of the classical approach via partial differential equations is an open question. The dynamics of a heavy storm in northern California which took place in January 1995 are being studied based on the ideas outlined in this section.

4 Summary, Conclusions, and Recommendations

A geometric framework for the description of complex hydrologic (geophysical) data has been reviewed. The method relies on the use of fractal-geometric techniques and in particular on the combination of fractal interpolation functions and multinomial multifractal measures. It has been illustrated that although the procedure appears to be just geometrical, it may also have a physical significance. This is because the two components that make up the method are being found of importance to understand nature and in particular turbulence. The physical realism of the outcomes produced by the procedure is further emphasized by the unexpected connection that plane-filling and space-filling fractal interpolating functions provide between "disorder" (turbulence) and "harmony"(Gaussian behavior).

Faithful representations for three high resolution storms based on the fractal-multifractal procedure have been presented in this work. Detailed statistical analysis of the real and predicted time series reveals that the predicted series not only preserve relevant statistical and multifractal characteristics of the original records, but also the overall geometric details of the highly intermittent observations. This implies that there is no need to separate trends and presumably unimportant small oscillations when dealing with rainfall records.

In fact, the results in this work suggest a new global perspective for understanding rainfall, a perspective in which major features and noisy details are captured jointly. Clearly, the analysis suggests that a stochastic framework for rainfall modeling may not be necessary.

It has been shown that the fractal-multifractal representation results in weighted projections which, depending on the procedures' surrogate parameters, may be classified as low-dimensional and chaotic, or as multi-dimensional and stochastic. Although the fractal-multifractal representation gives deterministic outcomes, none of these behaviors can be anticipated beforehand. In fact, having a chaotic or an stochastic character in the unique (and hence deterministic) derived measures is not trivial, but is clearly dependent on the degree of filtering that a fractal interpolation function does on the parent multifractal measure. The fact that some forms of chaotic and stochastic behavior may be obtained by the fractal-multifractal procedure suggests that such an approach, or a similar one based on weighted projections, may be key in understanding nature.

By means of some spatial simulations it has been argued that the fractal-multifractal approach may be used to: (i) represent rainfall's spatial patterns, and (ii) to study the space-time dynamics of storms. Clearly, the fractal-multifractal methodology, or a similar one, would be relevant in our ability to predict if dynamics are sufficiently nonlinear such that details matter. It seems certainly conceivable that a dynamic description may be developed based on geometric encodings of actual rainfall (hydrologic) data in space. This means, perhaps, bypassing the use of (stochastic) partial differential equations for relevant physical processes, and instead concentrating on the time evolution of surrogate geometric parameters of rainfall shapes which reflect the physico-chemical-biological processes taking place within the atmosphere. This particular issue is important in practice and deserves attention in the future.

It is clear to the author that the fractal-multifractal procedure may be applied to model a great variety of geophysical processes. If doing dynamics from geometry is found viable in hydrologic studies, it could also be applied to a great variety of other natural sciences. The proposed methodology is universal in the sense that it concentrates on geometry. After all, as James Clerk Maxwell said in 1879,

> ...geometry itself is part of the science of motion, and [that] it treats, not of the relations between figures already existing in space, but of the process by which these figures are generated by the motion ...This method of regarding geometrical figures seems to imply that the idea of motion underlies the idea of form ...

and therefore capturing geometry appears to be the key.

The search for efficient algorithms to properly describe real hydrologic data sets is vital. Of course the merit of this work will rest on our ability to solve an inverse problem in the least possible amount of time, specially when dealing with dynamics.

The results in this report suggest that the fractal-multifractal framework should be applied to represent not only high resolution rainfall records, but also more readily available data sets, i.e. those gathered every few minutes and which contain periods of no rain. Replacement of the parent multifractal measures with continuous domains by Cantorian measures represents the next idea to try in relation to these data sets.

5 References

Albano, A. M., Muench, J., and C. Schwartz. 1988. Singular-value decomposition and the Grassberger-Procaccia algorithm. *Physcal Review A* 38: 3017-3025.

Albano, A. M., Passamante, A., and M. E. Farrell. 1991. Using higher-order correlations to define an embedding window. *Physica D* 54: 85-97.

Barnsley, M. F. 1986. Fractal functions and interpolation. *Constructive Approximations* 2: 303-329.

Barnsley, M. F. 1988. *Fractals Everywhere.* Academic Press, New York.

Barnsley, M. F., J. Elton, D. Hardin, and P. Massopust. 1989. Hidden variable fractal interpolation functions. *SIAM Journal of Mathematical Analysis* 20(5): 1218-1242.

Benjamin, J. T., and C. A. Cornell. 1970. *Probability, Statistics, and Decision for Civil Engineers.* McGraw-Hill, New York.

Billingsley, P. 1983. The singular function of bold play. *American Scientist* 71: 392-397.

Bhattacharya, R. N., and E. C. Waymire. 1990. *Stochastic Processes with Applications.* John Wiley and Sons, New York.

Bras, R. L., and I. Rodriguez-Iturbe. 1985. *Random Functions and Hydrology.* Addison Wesley, Reading, Massachusetts.

Casdagli, M. 1989. Nonlinear prediction of chaotic time series. *Physica D* 35: 335-356.

Chhabra A. B., and R. V. Jensen. 1989. Direct determination of the $f(\alpha)$ singularity spectrum. *Physical Review Letters* 62(12): 1327-1330.

Chhabra A. B., C. Meneveau, R. V. Jensen, and K. R. Sreenivasan. 1989. Direct determination of the $f(\alpha)$ singularity spectrum and its application to fully developed turbulence. *Physical Review A* 40(9): 5284-5294.

Cressie, N. 1991. *Statistics for Spatial Data.* John Wiley and Sons, New York.

Crutchfield, J. P., and B. S. McNamara. 1987. Equations of motion from a data series. *Complex Systems* 1: 417-452.

Davies, P. (ed.). 1989. *The New Physics.* Cambridge University Press, Cambridge.

Dooge, J. C. I. 1986. Looking for hydrologic laws. *Water Resources Research* 22(9): 46S-58S.

Dubins, L. E., and L. J. Savage. 1960. Optimal gambling systems. *PNAS* 46: 1597-1598.

Eagleson, P.S. 1970. *Dynamic Hydrology.* McGraw-Hill, New York.

Eagleson, P. S. 1978. Climate, soil and vegetation 1-7, *Water Resources Research* 14(5): 705-776.

Feder, J. 1988. *Fractals.* Plenum Press, New York.

Feigenbaum, M. J. 1988. Universal behavior in nonlinear systems. *Los Alamos Science* Summer: 4-27.

Feller, W. 1968. *An Introduction to Probability Theory and Its Applications* vol 1., 3rd edition, John Wiley, London.

Foufoula-Georgiou, E., and P. Guttorp. 1986. Compatibility of continuous rainfall occurrence models with discrete rainfall observations. *Water Resources Research* 22(8): 1316-1322.

Fraser, A. M., and H. L. Swinney. 1986. Independent coordinates for strange attractors from mutual information. *Physical Review A* 33: 1134-1140.

Fraser, A. M. 1989. Information and entropy in strange attractors. *IEEE Transactions on Information Theory* 35: 245.

Georgakakos, K. P., and R. L. Bras. 1984. A hydrologically useful precipitation model. *Water Resources Research* 20(11): 1585-1596.

Georgakakos, K. P., A. A. Carsteanu, P. L. Sturdevant, and J. A. Cramer. 1994. Observation and analysis of midwestern rain rates. *Journal of Applied Meteorology* 33(12): 1433-1444.

Grassberger, P., and I. Procaccia. 1983. Measuring the strangeness of strange attractors. *Physica D* 9: 189-208.

Grassberger, P., and I. Procaccia. 1983. Estimation of the Kolmogorov entropy from a chaotic signal. *Physical Review A* 28: 2591-2593.

Grassberger, P. 1990. An optimized box-assisted algorithm for fractal dimensions. *Physics Letters A* 148: 63-68.

Gupta, V. K. 1973. *A stochastic approach to space-time modeling of rainfall. Technical Report on Natural Resource Systems* 18, University of Arizona, Tucson.

Guttorp, P. 1986. On binary time series obtained from continuous time point processes describing rainfall. *Water Resources Research* 22(6): 897-904.

Halsey, T. C., M. H. Jensen, L. P. Kadanoff, I. Procaccia and B. I. Shraiman. 1986. Fractal measures and their singularities: the characterization of strange sets. *Physical Review A* 33: 1141-1151.

Hentschel, H., and I. Procaccia. 1983. The infinite number of generalized dimensions of fractals and strange attractors. *Physica D* 8: 435-441.

Holley, R., and E. C. Waymire. 1992. Multifractal dimensions and scaling exponents for strongly bounded random cascades. *The Annals of Applied Probability* 2(4): 819-845.

Kavvas, M. L., and J. W. Delleur. 1981. A stochastic cluster model of daily rainfall sequences. *Water Resources Research* 17(4): 1151-1160.

Kennel, M. B, R. Brown and H. D. I. Abarbanel. 1992. Determining embedding dimension for phase-space reconstruction using a geometrical construction. *Physical Review A* 45(6): 3403-3411.

Lavallée, D., S. Lovejoy, D. Schertzer, and P. Ladoy. 1991. Nonlinear variability and Landscape topography: analysis and simulation. pp. 171-205. In L. De Cola and N. Lam (eds) *Fractals in Geography.* Prentice-Hall, New York.

Lesieur, M. 1990. *Turbulence in Fluids.* Kluwer Academic Publishers, Dordrecht, Holland.

Libchaber, A. 1982. Convection and turbulence in liquid helium I, *Physica B* 109 & 110: 1583-1589.

Lorenz, E. N. 1963. Deterministic nonperiodic flow. *Journal of the Atmospheric Sciences* 20: 130-141.

Lovejoy, S., and D. Schertzer. 1985. Generalized scale invariance in the atmosphere and fractal models of rain. *Water Resources Research* 21(8): 1233-1250.

Lovejoy, S., and D. Schertzer. 1990. Multifractals, universality classes and satellite and radar measurements of cloud and rain fields. *Journal of Geophysical Research* 95(D3): 2021-2034.

Mandelbrot, B. B. 1983. *The Fractal Geometry of Nature.* Freeman, San Francisco.

Mandelbrot, B. B. 1989. Multifractal measures especially for the geophysicist. pp. 1-42. In: C. H. Scholz and B. B. Mandelbrot (eds) *Fractals in Geophysics.* Birkhauser Verlag, Basel.

Marani, A., R. Rigon, and A. Rinaldo. 1991. A note on fractal channel networks. *Water Resources Research* 27(12): 3041-3049.

Marien, J. L., and G. L. Vandewielde. 1986. A point rainfall generator with internal storm structure. *Water Resources Research* 22(4): 475-482.

Meneveau, C., and K. R. Sreenivasan. 1987. Simple multifractal cascade model for fully developed turbulence. *Physical Review Letters* 59: 1424-1427.

Moon, F. C. 1987. *Chaotic Vibrations.* Wiley, New York.

National Research Council. 1991. *Opportunities in the Hydrologic Sciences*, 348 pp., National Academy Press, Washington, D. C..

National Research Council. 1991. *Spatial Statistics and Digital Image Analysis*, 234 pp., National Academy Press, Washington, D. C..

Otten, R. H. J. M., and L. P. P. P. van Ginneken. 1989. *The Annealing Algorithm.* Kluwer Academic Publishers, Boston.

Press, W. H., B. P. Flannery, S. A. Teukolsky, and W. T. Vetterling. 1989. *Numerical Recipes.* Cambridge University Press.

Provenzale, A., A. R. Osborne, and R. Soj. 1991. Convergence of the K_2 entropy for random noises with power law spectra. *Physica D* 47: 361-372.

Puente, C. E. 1991. Multinomial multifractals, fractal interpolators, and the Gaussian distribution. *Physics Letters A* 161: 441-447.

Puente, C. E. 1994. Deterministic fractal geometry and probability. *International Journal of Bifurcations and Chaos* 4(6): 1613-1629.

Puente, C. E., and A. Klebanoff. 1994. Gaussians everywhere. *Fractals* 2(1): 65-79.

Puente, C. E., and R. Lobato. 1994. Cantorian measures and temporal rainfall. *Annals Geophysicae* 12(II): C410.

Puente, C. E., and M. G. Juliao. 1994. Stochastic characteristics of deterministically generated multifractal measures. *Annals Geophysicae* 12(II): C518.

Puente, C. E. 1995. A new approach to hydrologic modeling: derived distributions revisited. *Journal of Hydrology.* In press.

Puente, C. E., and N. Obregón. 1995. A fractal-multifractal model of rainfall: three case studies. *Annals Geophysicae* 13(II): C468.

Puente, C. E., M. M. López, J. E. Pinzón, and J. M. Angulo. 1996. The Gaussian distribution revisited. *Advances in Applied Probability.* In press.

Rodriguez-Iturbe, I., V. K. Gupta, and E. Waymire. 1984. Scale considerations in the modeling of temporal rainfall. *Water Resources Research* 20(11): 1611-1619.

Rodriguez-Iturbe, I. 1986. Scale of fluctuation of rainfall models. *Water Resources Research* 22(9): 15S-37S.

Rodriguez-Iturbe, I., D. R. Cox, and V. Isham. 1987. Some models for rainfall based on stochastic point processes. *Proceedings of the Royal Society of London A* 410: 269-288.

Rodriguez-Iturbe, I., B. Febres de Power, and J.B. Valdes. 1987. Rectangular pulses point process models for rainfall: analysis of empirical data. *Journal of Geophysical Research* 92(D8): 9645-9656.

Rodriguez-Iturbe, I., B. Febres de Power, M. B. Sharifi and K. P. Georgakakos. 1989. Chaos in rainfall. *Water Resources Research* 25(7): 1667-1675.

Schertzer, D., and S. Lovejoy. 1987. Physical modeling and analysis of rain and clouds by anisotropic scaling multiplicative processes. *Journal of Geophysical Research* 92(D8): 9693-9714.

Schertzer, D., and S. Lovejoy. 1989. Nonlinear variability in geophysics: multifractal analysis and simulation. In L. Pietronero (ed) *Fractals' Physical Origin and Properties.* Plenum Press, New York.

Smith, J. A., and A. F. Karr. 1983. A point process model of summer season rainfall occurrences. *Water Resources Research* 19(1): 95-103.

Smith, J. A., and A. F. Karr. 1985. Statistical inference for point process models of rainfall. *Water Resources Research* 21(1): 73-79.

Smith, J. A. 1987. Statistical modeling of daily rainfall occurrences. *Water Resources Research* 23(5): 885-893.

Sreenivasan, K. R. 1991. Fractals and multifractals in fluid turbulence. *Annual Reviews in Fluid Mechanics* 23: 539-600.

Todorovic, P. 1968. A mathematical study of precipitation phenomena. *Report CER 67-68PT65.* Engineering Research Center, Colorado State University, Fort Collins.

Valdes, J. B., I. Rodriguez-Iturbe, and V. K. Gupta. 1985. Approximations of temporal rainfall from a multidimensional model. *Water Resources Research* 21(8): 1259-1270.

Waymire, E., and V. K. Gupta. 1981. The mathematical structure of rainfall representations, 1-3. Some applications of the point process theory to rainfall processes. *Water Resources Research* 17(5): 1261-1294.

Wolf, A., Swift, J. B., Swinney, H., and J. A. Vastano. 1985. Determining Lyapunov exponents from a time series. *Physica D* 16: 286-317.

Zhou, J. L., and A. L. Tits. 1993. Nonmonotone line search for minimax problems. *Journal of Optimization Theory and Applications* 76: 455-476.